Response to referees: Chemical Characterisation of Water-soluble Ions in Atmospheric Particulate Matter on the East Coast of Peninsular Malaysia

The authors addressed part of the comments while some critical comments were not satisfactorily responded or fully explained.

As for comment #4, the authors replied that "the levels of K+ do not rule out the influence of biomass burning on a regional/national scale." At least, the authors should check whether there were biomass burning events on a regional/national scale by looking at fire hotspots from satellites. Secondly, the authors responded that "Biomass burning aerosol in the wider region will have undergone atmospheric processing and dispersion prior to arrival at the measurement site, potentially lowering K+ levels and raising the concentration of secondary species." If this statement is correct, sulfate should also be subject to the similar process as the authors found sulfate derived from long-range transport. However, the concentrations of sulfate maintained at high levels and I didn't see an obvious dispersion effect.

There is one paper published in Scientific Reports that showed that the signal of biomass burning could be detectable from the north pole to the south pole from cruise measurement. The concentrations of K+ less than 1ug/m3 were likely representative of the background signal of biomass burning emissions over the region but didn't necessarily point to the biomass burning activities in a wider region.

The authors have taken the reviewers advice and investigated the occurrence of fires in the region surrounding the site using data obtained from the moderate-resolution imaging spectroradiometer (MODIS) instrument on board the NASA Terra satellite (Giglio et al. 2003). Fire maps were accessed *via* the global forest watch website (GFW, 2018) and are shown in Figure S4 for the measurement period discussed in this paper. It is clear that there is widespread biomass burning throughout SE Asia during our measurements. Lines 562-565 have been amended to explain this point more clearly. However, the most important point of this discussion in the manuscript is the observed correlation of $nssK^+$ with the oxalate ion, and the $nssK^+$/oxalate ratio. Whilst K^+ levels may be relatively low (less than 1 μg m^{-3}), there is a strong positive correlation between $nssK^+$ and oxalate, and a low $nssK^+$/oxalate ratio. This indicates that $nssK^+$ from biomass burning (which has been observed in the wider region) may be an important source of secondary oxalate, rather than a primary source (lines 564 – 572).

Comment #5: The authors explained the high concentrations of sulfate in Cluster 5 came from higher altitudes in a low pressure system (no more explanations were offered). Then in the response to Comment #9, the authors explained that the concentrations of Cl- were low, which were also due to the air masses at high altitudes. Those inconsistent analysis and discussions in different sections of the manuscript are common in this study.

This point has been explained more clearly (lines 416 - 425). For clusters 1 – 4, the highest SO_4^{2-} concentrations are seen when air masses arriving at the site come from low altitudes and have significant continental influence from industrialised regions of East Asia. The lowest SO_4^{2-} concentrations are seen for marine air masses that have passed over the South China Sea.

Cluster 5 shows very different behaviour. We disagree that we have been inconsistent in our discussion and have presented the data clearly. The air masses in cluster 5 arriving at the site are not a result of north-easterly winds from East Asian countries travelling across the South China Sea. Instead, there is evidence of a cyclonic weather system off the coast of the island of Borneo over the South China Sea. The air masses in cluster 5 arrived during the final 24-hour period of the measurement campaign and only one SO_4^{2-} measurement is available (18.1 ug m^{-3}). It is not possible to fully understand the nature of air masses from this different region without further measurements.

Figure 6 & Figure 7,8

The pollution rose plot (Figure 6) of SO2 shows that there were almost no prevailing winds from the north and high concentrations of SO2 mainly came from the west and south. But the backward trajectories analysis (Figures 7,8) dominantly derived from the north. I'm really confused that how could the analysis of meteorological conditions differed so much.

The author has misunderstood the data that is presented in Figure 6 (now Figure 5). As explained in lines 362 – 372, the pollution rose plot of SO2 (Fig 6) only showed SO_2 concentrations above 5 ppb *i.e.* the elevated SO_2 events. The pollution rose excluded SO_2 concentrations below 5 ppb.

The plot showed that most of the spikes in SO_2 were observed in calmer conditions when the air arriving at the site had passed over nearby land to the south west of Bachok.

A direct comparison with wind directions presented in figures 7 and 8 is not appropriate because figures 7 and 8 represent the back trajectories across the entire measurement period, rather than solely during the high SO_2 events.

The trajectories focus on long-range transport and represent the dominant overall meteorological conditions, which were strong north-easterlies from East Asia and the South China Sea. The dominance of north-easterlies has been further illustrated in Figure S2 in the Supplement, which shows hourly wind rose plots averaged across the measurement campaign.

An additional pollution rose has been added to Figure 6 to make this point clear. The left panel represents recorded SO_2 concentrations ≥ 5 ppb and the right panel represents all SO_2 data recorded during the measurement period.

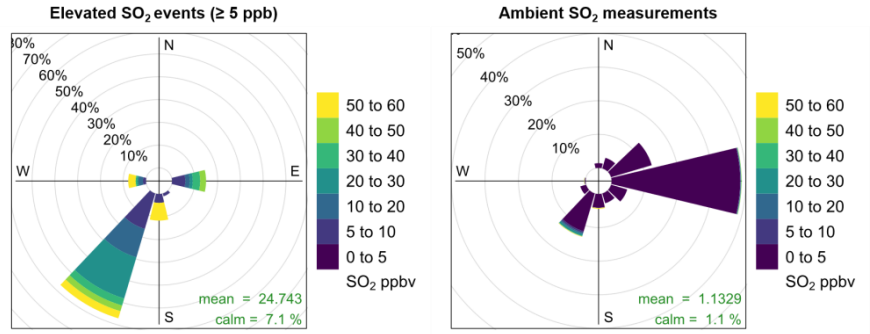

Overall, I didn't see great improvement of the presentation quality of the manuscript. Both referees requested improving the quality of figures and descriptions while the authors didn't take the suggestions. Data analysis is presented in a very simple manner and a lot of the discussions are based on hypothesis without firm evidence or other supportive data. Most importantly, contradictions were often found which makes the manuscript unreadable. I personally don't think the current version of this manuscript meets the quality of the journal.

The quality of figures and descriptions has been significantly improved throughout the entire manuscript. The authors has improved the quality of discussions where necessary, and clarified the misunderstandings surrounding Figures 6, 7 and 8. The author believes that this version of the manuscript meets the quality of ACP.

Chemical Characterisation of Water-soluble Ions in Atmospheric Particulate Matter on the East Coast of Peninsular Malaysia

Naomi J. Farren[1], Rachel E. Dunmore[1], Mohammed Iqbal Mead[2], Mohd Shahrul Mohd Nadzir[3,4], Azizan Abu Samah[5], Siew-Moi Phang[5], Brian J. Bandy[6], William T. Sturges[6], Jacqueline F. Hamilton[1].

[1]Wolfson Atmospheric Chemistry Laboratories, Department of Chemistry, University of York, York, YO10 5DD, UK.
[2]Centre for Atmospheric Informatics and Emissions Technology, School of Energy, Environment and Agrifood/Environmental Technology, Cranfield University, Cranfield, UK.
[3]Centre for Tropical Climate Change System (IKLIM), Institute of Climate Change, Universiti Kebangsaan Malaysia, 43600 Bangi, Selangor, Malaysia.
[4]School of Environmental Science and Natural Resources, Faculty of Science and Technology, Universiti Kebangsaan Malaysia, 43600 Bangi, Selangor Darul Ehsan, Malaysia.
[5]Institute of Ocean and Earth Sciences, University of Malaya, Kuala Lumpur, Malaysia.

Formatted: Superscript

[6]Centre for Ocean and Atmospheric Sciences, School of Environmental Sciences, University of East Anglia, Norwich, UK.

Correspondence to: Jacqueline F. Hamilton (jacqui.hamilton@york.ac.uk)

Abstract.

Air quality on the east coast of Peninsular Malaysia is influenced by local anthropogenic and biogenic emissions, as well as marine air masses from the South China Sea and aged emissions transported from highly polluted East Asian regions during the winter monsoon season. An atmospheric observation tower has been constructed on this coastline at the Bachok Marine and Atmospheric Research Station. Daily $PM_{2.5}$ samples were collected from the top of the observation tower over a 3-week period, and ion chromatography was used to make time-resolved measurements of major atmospheric ions present in aerosol. SO_4^{2-} was found to be the most dominant ion present, and on average made up 66% of the total ion content. Predictions of aerosol pH were made using the ISOROPPIA-II thermodynamic model and it was estimated that the aerosol was highly acidic, with pH values ranging from -0.97 to 1.12. A clear difference in aerosol composition was found between continental air masses originating from industrialised regions of East Asia and marine air masses predominantly influenced by the South China Sea. For example, elevated SO_4^{2-} concentrations and increased Cl^- depletion was observed when continental air masses that had passed over highly industrialised regions of East Asia arrived at the measurement site. Correlation analyses of the ionic species and assessment of ratios between different ions provided an insight into common sources and formation pathways of key atmospheric ions, such as SO_4^{2-}, NH_4^+ and $C_2O_4^{2-}$. To our knowledge, time-resolved measurements of water-soluble ions in $PM_{2.5}$ are virtually non-existent in rural locations on the east coast of Peninsular Malaysia; overall this dataset contributes towards a better understanding of atmospheric composition in the Maritime Continent, a region of the tropics that is vulnerable to the effects of poor air quality, largely as a result of rapid industrialisation in East Asia.

1 Introduction

The tropical Maritime Continent, a region in Southeast Asia between 10° S – 20 °N and 90° - 150° E, is a complex distribution of islands and peninsulas, and incorporates countries such as Malaysia, Indonesia, the Philippines and Papua New Guinea (Neale and Slingo, 2003). It lies within a tropical warm pool that extends eastwards from the Indian Ocean to the Western Pacific, and is home to some of the warmest ocean temperatures in the world. Tropical regions such as the Maritime Continent are of central importance for the chemistry-climate system (Carpenter et al., 2010). For example, high photochemical activity in these regions means that global atmospheric lifetimes of key atmospheric species, such as methane and ozone, are controlled by destruction rates in the tropics (Lawrence et al., 2001; Bloss et al., 2005). In terms of ocean productivity, the observed decrease in primary productivity in low-latitude oceans has been linked to a reduced availability of nutrients for phytoplankton growth, caused by changes in upper-ocean temperature and stratification (Behrenfeld et al., 2006). Furthermore, the wind circulation system in the Maritime Continent is influenced by seasonal Asian monsoons, which are controlled by the natural oscillation of the intertropical convergence zone (ITCZ). During the northern hemisphere winter, a large anticyclone forms

over Siberia each year, creating strong north-easterly monsoon winds in the South China Sea (Northeast Monsoon). These strong north-easterlies can transport air masses from rapidly developing East Asian countries (*e.g.* China, Japan, Vietnam, North and South Korea) across the South China Sea to the Maritime Continent (Zhang et al., 1997; Garreaud, 2001; Oram et al., 2017). In addition, cold surge events occur regularly throughout the winter monsoon season and last several days. Cold surges occur as a result of a south-easterly movement of the anticyclone, and are characterised by cold air masses over Southern China and strengthening of the north-easterly monsoon winds in the South China Sea (Zhang et al., 1997). The transport of pollution from East Asia to the tropics during the monsoon season, particularly during cold surges, means that rural areas such as the east coast of Peninsular Malaysia are potentially at an elevated risk of the detrimental effects of poor air quality.

Tropical regions are highly important for atmospheric research, and whilst long-term atmospheric observations exist (Robinson et al., 2014; Pyle et al., 2011), there are fewer measurements than in the mid and high-latitudes. The Bachok Marine and Atmospheric Research Station (6.00892° N, 102.42504° E) has been set up on the east coast of Peninsular Malaysia and is ideally located for studying the outflow of these highly industrialised regions, and for investigating the interaction with cleaner air in the Southern hemisphere. The research station forms part of the Institute of Ocean and Earth Sciences at the University of Malaya (UM), and is located approximately 30 km away from Kota Bharu. An atmospheric observation tower facing the South China Sea has been constructed at the research station; this has been built for the specific purpose of monitoring long-range transported pollution, air sea exchange and coastal meteorology. The research station is working towards designation as a regional Global Atmospheric Watch (GAW) centre, which will be a valuable addition to the network of other global and regional GAW sites in the Maritime Continent, as shown in Fig. 1 (gawsis.ch, 2017).

Figure 1: Location of the Bachok research station (BRT) and the global ~~(green pins)~~ and regional ~~(blue pins)~~ GAW sites in the Maritime Continent; Danum Valley in Malaysia (DMV), Bukit Kototabang in Indonesia (BKT), Manila in Philippines (MNI), Songkhla in Thailand (SKH), Tanah Rata in Malaysia (TAR), Petaling Jaya in Malaysia (PJM) and Singapore (SIN) (gawsis.ch, 2017). ~~The red pin shows the location of the Bachok Marine and Atmospheric Research Station. Map created using google maps (google.com, 2017).~~

In January and February 2014, an instrument demonstration campaign was carried out to assess the capabilities of the new research station. This was funded by the Natural Environment Research Council (NERC) and UM and involved several UK universities, as well as the National Centre for Atmospheric Science (NCAS), UM and the Malaysia Meteorological Department (MMD). As part of this study, Dunmore et al. (2016) used a specialised multi-dimensional gas chromatography technique to accurately measure atmospheric mixing ratios of C_5-C_{13} volatile organic compounds (VOCs)~~VOC species~~ with a wide range of functionalities. Furthermore, Dominick et al. (2015) characterised the particulate matter in Bachok by studying the influence of north-easterly winds on the patterns of particle mass and particle number concentration size distributions. Both

studies highlighted the fact that the site is influenced by a mixture of local anthropogenic and biogenic emissions, clean marine air masses, and aged emissions transported from East Asia.

To extend upon these studies, it is important to investigate atmospheric aerosol composition in the Bachok region. A better understanding of aerosol chemical composition is essential as aerosols play an important role in atmospheric processes and climate change. For example, aerosols can modify the global radiation budget both directly, by scattering and absorbing solar radiation, and indirectly, by altering cloud properties and lifetime (Charlson et al., 1991). The strength of these direct and indirect effects depends partly on the particle concentration and size distribution, but also on the chemical composition.

There are a limited number of studies that focus on particulate matter composition on the east coast of Peninsular Malaysia, and to our knowledge the composition of ionic species has not been determined at any rural locations along this coastline. For example, Tahir et al. (2013) studied the composition of major elements and water-soluble ionic species in $PM_{2.5}$ and PM_{10} samples on the east coast of Peninsular Malaysia, but the samples were collected at an urban coastal city, Kuala Terengganu. This study used principal component analysis to determine the main sources of both fine and coarse particles, which were found to be soil dust, marine aerosol, vehicle exhaust, secondary aerosol, road dust and biomass burning. In addition, Ismail et al. (2016) studied PM_{10} concentrations in three major cities (Kota Bahru, Kuala Terengganu and Kuantan) on the east coast of Peninsular Malaysia between 2006 and 2012. The study showed that during the Northeast Monsoon, the air arriving at the sites had originated from China and the Philippines and travelled over the South China Sea. During the Southwest Monsoon, the air came from Indonesia *via* the Straits of Malacca. Over the 6-year period, it was found that the atmospheric PM_{10} mass was directly proportional to the rate of urbanization in each of the three cities.

In this study, measurements of water-soluble ions in atmospheric aerosol at a rural coastal location on the east coast of Peninsular Malaysia are presented. Analysis of temporal variation of different ionic species has been carried out, and backward air mass trajectories have been used to determine the influence of air mass origin on aerosol composition. Correlation analyses of the ionic species and assessment of ratios between different ions has provided an insight into common sources and formation pathways of key atmospheric ions.

2 Experimental

2.1 Sample collection and extraction

Thirty $PM_{2.5}$ samples were collected at the Bachok Marine and Atmospheric Research Station (6.00892° N, 102.42504° E) between 18-01-2014 and 06-02-2014. The samples were collected at the top of an atmospheric observation tower (18 m height) using a high volume air sampler (Ecotech HiVol 3000, Victoria, Australia) operating at 1.13 m^3 min^{-1} over 24 h sampling intervals. The tower is located on the coastline of the South China Sea and is within 100 m of the shore. A 3-day intensive

measurement period was in operation between midday (local time) on 30-01-2014 and midday on 02-02-2014, in which filters were collected every 4-8 hours. The quartz fibre filters (20.3 × 25.4 cm) supplied by Whatman (Maidstone, UK) were prebaked at 550 °C for a minimum of 12 h prior to sample collection. After sample collection, the filters were wrapped in aluminium foil and stored at -18 °C until analysis. To prepare the samples for analysis, 5.7 cm^2 of each sample was dissolved in 2 mL milli-Q water and sonicated for 30 min at room temperature. The extract was filtered using a Millex-GP 33 mm diameter hydrophilic syringe filter with a pore size of 0.22 µm (Millipore UK Limited, Watford, UK) and made up to a final volume of 2.5 mL.

2.2 Eluents and analytical standards

Ultrapure milli-Q water (18 MΩ cm^{-1}) from an ELGA LabWater purification system was used to prepare all the required eluents and analytical standards. A 20 mM solution of methanesulfonic acid was used as the eluent for cation exchange chromatography and for anion exchange chromatography, a solution of 8 mM Na_2CO_3/1 mM $NaHCO_3$ was prepared. Using a variety of salts and organic acids, individual analytical standards containing 500 ppm of each target ion (Cl^-, NO_2^-, NO_3^-, PO_4^{3-}, SO_4^{2-}, $CH_3SO_3^-$, $C_2O_4^{2-}$, Na^+, NH_4^+, K^+, Mg^{2+} and Ca^{2+}) were prepared in milli-Q water. The salts and organic acids were purchased from either Sigma-Aldrich Ltd. (Dorset, UK) or Fisher Scientific Ltd. (Loughborough, UK).

2.3 Chromatographic analysis

Chromatographic analysis was carried out using a Thermo Scientific Dionex ICS-1100 ion chromatography system equipped with an AS-DV autosampler. The column configuration used for anion exchange consisted of an IonPac AG14A guard column (4 × 50 mm) and an IonPac AS14A analytical column (4 × 250 mm). Cation exchange chromatography was performed using an IonPac CG12A guard column (4 × 50 mm) and an IonPac CS12A analytical column (4 × 250 mm). ASRS 300 and CSRS 300 self-regenerating suppressors (4 mm) were used for anion and cation exchange respectively. All columns and suppressors were supplied from Thermo Scientific Dionex. The run times for the anion and cation separations were 18 and 15 min respectively. The suppressor current was 45 mA for anion exchange mode, and 59 mA for cation exchange mode. For all separations, the instrument was operated in isocratic mode at a flow rate of 1 mL min^{-1} and a column oven temperature of 30 °C. The injection volume was 100 µL and the data collection rate was 5 Hz. The system relied on a DS6 heated conductivity cell for ion detection and all data was analysed using Thermo Scientific Chromeleon 7.1 Chromatography Data System software.

2.4 Method validation

Using isocratic elution methods for both cation and anion exchange chromatography, the target ions were successfully separated. Recovery tests were performed by spiking 5.7 cm^2 of quartz fibre filters (Whatman, Maidstone, UK) with 1 µg of each target ion (20 µL of a 50 ppm mixed ion solution). Prior to spiking, the filters were prebaked at 550 °C for 6 hours and

wrapped in aluminium foil and stored at -18 °C until required. The spiked filters were dissolved in 2 mL of milli-Q water and sonicated for 30 min at room temperature. The extract was filtered using a Millex-GP 33 mm diameter hydrophilic syringe filter with a pore size of 0.22 µm (Millipore UK Limited, Watford, UK) and made up to a final volume of 2.5 mL. The recovery of the target ions from the filter papers ranged from 74.5% to 98.2% for the target anions, and 78.3% to 87.3% for the target cations, with the exception of Ca^{2+} for which a recovery level of 123.3% was calculated. Recovery tests were carried out in triplicate and $\%RSD_{rec}$ remained below 8% for all the ions. The recovery of Ca^{2+} should not have exceeded 100% and the result may be attributed to inconsistencies in the amount of Ca^{2+} present on the blank filter, or due to Ca^{2+} contamination during sample collection or storage. 100% recovery was assumed for Ca^{2+} during the data analysis process. Further details of the individual recovery levels and associated errors can be found in the Supplement (Table S1). Procedural blanks were also carried out using quartz fibre filters (5.7 cm^2) and blank subtractions were applied to any target ions found in detectable amounts. The blank peak areas for each ion and average blank contribution to field samples over the entire sampling period are provided in the Supplement, Table S1. The main instrumental parameters of the IC system were evaluated and are also detailed in the Supplement (Table S2). Instrumental limits of detection (LODs) and limits of quantification (LOQs) were calculated according to the EPA protocol 40 CFR 136; multiplying the standard deviation (N = 10, 5 ng for cations, 25 ng for anions) by the Student t-value (N = 10, 95% confidence interval) gave the LOD, and multiplying the standard deviation by 10 gave the LOQ (EPA, 2017; Ripp, 1996). For anion exchange chromatography, LODs and LOQs were in the range 5.5 – 21.0 ng and 25.3 – 144.2 ng respectively. For cation exchange chromatography, the LODs ranged from 0.5 to 2.1 ng and the LOQs ranged from 2.5 to 6.1 ng. On average, the instrument precision ($\%RSD_{ins,}$ n = 10) was 4.2% for the target cations and 12.8% for the target anions. Total errors were estimated by combining errors with the instrument and the recovery process and remained below 15.4% for all ions except NO_3^- (22.6%).

2.5 Additional measurements

Individual volatile organic compounds (VOCs) were measured using a combined heart-cut and comprehensive two-dimensional gas chromatography system (GC-GC×GC); a detailed description of the instrument design is provided in a separate study (Dunmore et al., 2016). Measurements of NO and NO_2 were performed using a two channel TE42i commercial gas analyser (Thermo Scientific, MA, USA), and SO_2 measurements were made using a Thermo Scientific 43i SO_2 analyser. Meteorological data from the nearest meteorological station, the Sultan Ismail Petra Airport (6.17208° N, 102.29288° E), was accessed from the Integrated Surface Database (NOAA, 2003). Hourly measurements of wind direction, wind speed, air temperature, dew point, atmospheric pressure and relative humidity were obtained. 10-day backward air mass trajectories arriving at the sampling site were run every 3 hours throughout the entire measurement period. A receptor height of 10 m was chosen to represent the measurements made on the sampling tower. The trajectories were computed using the Hybrid Single-Particle Lagrangian Integrated Trajectory (HYSPLIT) model (Stein et al., 2015; Draxler, 1999; Draxler and Hess, 1998, 1997), and the data was analysed using the openair package in RStudio (Carslaw and Ropkins, 2012; Carslaw, 2015).

2.6 ISORROPIA-II model

Predictions of aerosol pH were made using the ISORROPIA-II thermodynamic equilibrium model. Although these models produce better results when gas phase measurements such as NH_3 and HNO_3 are available, it is possible to use the ion measurements obtained in this study to make a prediction of aerosol pH (Fountoukis and Nenes, 2007). Calculations were made in 'reverse mode', in which known quantities are temperature, relative humidity, and particle phase concentrations of NH_4^+, SO_4^{2-}, Na^+, Cl^-, NO_3^-, Ca^{2+}, K^+ and Mg^{2+}. ISOROPPIA-II assumes that the particles are internally mixed; this is a reasonable assumption for this study, as relative humidity was high (average = 77%) and the aerosol arriving at the measurement site is often aged. The aerosol was assumed to be thermodynamically stable *i.e.* the aerosol can exist as both solid and liquid, and salts are able to precipitate if the aqueous phase becomes saturated with respect to them. The ambient temperature and relative humidity data were taken from the measurements made nearby at the Sultan Ismail Petra airport. It is likely that these measurements are representative of the Bachok research station, as further investigation of data from two other meteorological stations showed that temperature and relative humidity remain consistent along the coastline.

3 Results and discussion

3.1 Bachok demonstration campaign

The filter samples were collected at the Bachok atmospheric observation tower. The Bachok district, located in the state of Kelantan, is a rural area and the primary economic activity comes from tobacco and kenaf plantations. Other agrarian activities in the wider Kelantan region include the production of rice and rubber, as well as additional economic activities such as livestock rearing and fishing. ~~Figure~~ Fig. 2 shows the 7-day backward air mass trajectories arriving at the measurement site during the demonstration campaign, with each trajectory coloured by the mean altitude ~~of the air mass~~ (m). For comparison with pollutant trends later in this study, the trajectories have been separated into two plots according to their mean height. As expected during the winter months, the strong anticyclone system known as the Siberian High led to the arrival of north-easterly onshore winds along the east coast of Peninsular Malaysia. Some of the air masses experienced a significant continental influence from highly industrialised countries such as China, Japan, North and South Korea and the island of Taiwan, whilst other air masses had a stronger marine influence from both the East China Sea and the South China Sea.

Figure 2: 7-day HYSPLIT backward air mass trajectories centred on the Bachok Marine and Atmospheric Research Station between 18-01-2014 and 07-02-2014. ~~The back trajectories are~~Each trajectory is coloured by the mean altitude ~~of the air mass~~ (m). Trajectories with a mean height of 80 m or below are shown in the left panel and trajectories with a mean height greater than 80 m are shown in the right panel. ~~Plot constructed using the openair package in RStudio (Carslaw and Ropkins, 2012; Carslaw, 2015).~~

Although there was no reliable meteorological data recorded at the measurement site during the demonstration campaign, data from a nearby meteorological station was available. The station is located approximately 23 km away at the Sultan Ismail Petra airport in Kota Bharu, as shown in Fig. S1 (Supplement). Whilst the meteorological data from the airport will not be exactly representative of the measurement site, the patterns in wind direction are consistent with observations made by the field scientists during the campaign. In addition, during a study of the influence of Northeast Monsoon cold surges on air quality in Southeast Asia, Ashfold et al. (2017) used meteorological data from three locations that they believed to lie in the path of cold surges during the Northeast Monsoon, offering the best possibility of observing a cold surge influence on air pollution. These sites were in Kota Bharu (102.247° E, 6.141° N), Kuala Terengganu (103.118° E, 5.308° N) and Kemaman (103.428° E, 4.271° N); this provides further confirmation that data from the Sultan Ismail Petra airport site is suitable for evaluating broad scale transport at the Bachok measurement site. Fig. S2 in the Supplement shows average hourly wind speed and wind direction conditions across the entire duration of the measurement campaign (18-01-2014 to 06-02-2014). On most days, gentle south westerlies from the land (Peninsular Malaysia) were observed in the early hours of the morning, through to around 11 am. At this stage, a dramatic shift in wind direction occurred, and until around 19:00 a strong onshore breeze from the north east (South China Sea) was observed. From 20:00 to the early hours of each morning, a calmer sea breeze predominantly from the east was seen. Hourly VOC measurements were conducted at the measurement site, and the development of a sea breeze at approximately 11:00 dramatically influenced the diurnal profiles of the measured species (Fig. S3, Supplement). In the morning, when the air being sampled was coming over the land, high levels of NO, NO_2 and anthropogenic VOCs such as toluene and C_{10} aliphatics were observed; the main source of these species was local burning of waste (Dunmore et al., 2016). When the sea breeze developed the concentration of these species dropped significantly.

3.3 Composition of water-soluble ions in atmospheric aerosol

3.3.1 Aerosol composition and determination of non-sea salt and sea salt components

The total concentration of measured water-soluble ions in the $PM_{2.5}$ during the campaign ranged from 8.06 to 27.0 µg m^{-3}, with an average concentration of 16.2 µg m^{-3}. Table 1 shows the mean and maximum water-soluble ion concentrations measured throughout the campaign, and Fig. 3~~ures 3 and 4~~ show~~s~~ time series for all the ions measured in the aerosol.

Table 1: Mean and maximum ion concentrations measured throughout the measurement period. The average % mass contribution of each ion to the total measured ions is included, as well as the % of samples in which each target ion is found (%Qt).

Figure 3: Time series of water-soluble ions~~SO_4^{2-}, NH_4^+, Na^+, Cl^-, NO_3^- and NO_2^- concentration~~ (µg m^{-3}) measured during the Bachok demonstration campaign (18-01-2014 to 07-02-2014). ~~Yellow shaded areas represent the time between sunrise and sunset (local).~~

~~**Figure 4: Time series of PO_4^{3-}, Ca^{2+}, Mg^{2+}, K^+, $C_2O_4^{2-}$ and $CH_3SO_3^-$ concentration (µg m^{-3}) during the Bachok demonstration campaign (18-01-2014 to 07-02-2014). Yellow shaded areas represent the time between sunrise and sunset (local).**~~

As the composition of the water-soluble ions present in aerosol collected at the Bachok site was influenced by both marine and continental sources, it is useful to make an estimation of non-sea salt (*nss*) and sea salt (*ss*) components, using Eq. (1) – Eq. (4). Total Na^+ and Ca^{2+} concentrations have been measured in this study, and the mean Ca^{2+}/Na^+ ratio in the crust and mean Ca^{2+}/Na^+ ratio in seawater have been estimated as 1.78 *w/w* and 0.038 *w/w* respectively (Bowen, 1979).Therefore it is ~~it~~ possible to solve Eq. (1) – Eq. (4) simultaneously for *ss*Na^+, *nss*Na^+, *ss*Ca^{2+} and *nss*Ca^{2+} (Boreddy and Kawamura, 2015). Furthermore, the resulting estimate of *ss*Na^+, which can be used as a sea spray marker, can also be used to predict the contribution of *nss*SO_4^{2-} and *nss*K^+ in the aerosol, as shown in Eq. (5) and Eq. (6) respectively. Whilst there may be some uncertainty in the mean Ca^{2+}/Na^+ crustal ratio, due to challenges associated with predicting the composition of the crust (Bowen, 1979), this approach provides more accuracy than simply using total Na^+ as a sea spray marker.

$$ssNa^+ = Na^+ - nssNa^+ \quad (1)$$

$$nssNa^+ = nssCa^{2+} \cdot \left(\frac{Ca^{2+}}{Na^+}\right)_{crust} \quad (2)$$

$$nssCa^{2+} = Ca^{2+} - ssCa^{2+} \quad (3)$$

$$ssCa^{2+} = ssNa^+ \cdot \left(\frac{Ca^{2+}}{Na^+}\right)_{sea\ water} \quad (4)$$

$$nssSO_4^{2-} = SO_4^{2-} - 0.253 \cdot ssNa^+ \quad (5)$$

$$nssK^+ = K^+ - 0.037 \cdot ssNa^+ \quad (6)$$

~~Figure~~ Fig. ~~5~~ 4 shows a series of stacked bar~~pie~~ charts to summarise the average mass composition of water-soluble ions in atmospheric aerosol, and the distribution of non-sea salt and sea salt components. The results show that the water-soluble ion fraction of the aerosol is dominated by SO_4^{2-}, which on average made up 65.6% of the total ion content by mass. NH_4^+ and NO_3^- concentrations were significantly lower, with mean concentrations of 1.69 and 0.61 µg m^{-3} respectively. Na^+ and Cl^- made up 11.1% of the total ion content, and 75% of the measured Na^+ was attributed to *ss*Na^+. The average concentrations of *nss*K^+ and *nss*Ca^{2+} were 0.30 and 0.09 µg m^{-3} respectively; these ions can be used as tracers for biomass burning (*nss*K^+) and atmospheric dust (*nss*Ca^{2+}). NO_2^- and $CH_3SO_3^-$ were the least abundant ions, with average concentrations of 0.05 and 0.08 µg m^{-3}. The two ions were only observed in a subset of samples; $CH_3SO_3^-$ was quantified in 67% of samples and quantification of NO_2^- was only achieved in 23% of samples.

Figure ~~5~~4: Stacked bar chart~~Pie chart~~ to show the average composition of water-soluble ions in aerosol collected at the Bachok research station (~~upper~~ left panel) and ~~pie~~ stacked bar charts to show the percentage of non-sea salt and sea salt fractions of Ca^{2+}, K^+, Na^+, SO_4^{2-}, ~~K^+, Ca^{2+}~~ (~~lower~~right panel, left to right).

Formatted: Superscript

Formatted: Superscript

3.3.2 Sources and formation of sulfate (SO_4^{2-})

The average SO_4^{2-} concentration during the measurement campaign was 10.7 µg m^{-3}, with a maximum concentration of 20.8 µg m^{-3} recorded. The formation of SO_4^{2-} in the particle phase occurs when emitted SO_2 is oxidised by OH in the gas phase, or by O_3 or H_2O_2 in the aqueous phase (Fisher et al., 2011). The most dominant anthropogenic sources of SO_2 include fuel and industrial emissions, as well as open biomass burning.

By using *ss*Na^+ as a sea spray marker to determine non-sea salt and sea salt components of the aerosol, it was found that on average 96% of the measured SO_4^{2-} was *nss*SO_4^{2-}, and only 4% of the SO_4^{2-} was from sea salt. As a potential biogenic source of *nss*SO_4^{2-} is DMS emissions from marine biota, and the main atmospheric source of MSA is the oxidation of DMS, it is possible to use the MSA^-/*nss*SO_4^{2-} ratio as a tracer to assess the contribution of biogenic sources to *nss*SO_4^{2-} in the atmosphere (Legrand and Pasteur, 1998). In this study, MSA^- concentrations ranged from 0.02 to 0.22 µg m^{-3}, with an average concentration of 0.08 µg m^{-3}. As a result, the MSA^-/*nss*SO_4^{2-} ratio ranged from 1.6×10^{-3} to 2.2×10^{-2}, with an average value of 8.0×10^{-3}. These values are low compared to MSA^-/*nss*SO_4^{2-} ratios recorded at remote sites; for example, a MSA^-/*nss*SO_4^{2-} mean mass ratio of 7×10^{-2} has been measured on Fanning Island and American Samoa (Savoie and Prospero, 1989). The lower ratios recorded in Bachok suggest the majority of *nss*SO_4^{2-} at the site originates from anthropogenic sources.

As previously discussed, a study by Dunmore et al. (2016) revealed that levels of NO_x and anthropogenic VOCs at the Bachok measurement site were significantly higher when the air being sampled had passed over nearby land, and dropped significantly at around 11 am when a sea breeze developed. This indicated that air quality in Bachok is influenced by local sources of pollution, such as vehicle emissions and burning domestic waste. Pollution rose plots (Fig. 5) show the relationship between wind direction/speed and SO_2 concentration at the Bachok measurement site. The left panel shows recorded SO_2 concentrations ≥ 5 ppb and for comparison, the right panel shows all SO_2 data recorded during the measurement period. SO_2 concentrations < 5 ppb have been excluded from the left panel plot to further investigate the meteorological conditions when the spikes in SO_2 concentration occur. In the lower right corner of each pollution rose, 'mean' represents the mean SO_2 concentration and 'calm' represents the fraction of data that cannot be attributed to a specific wind direction. During the elevated SO_2 periods (≥ 5 ppb), weak south westerlies dominated and the average wind speed was 1.1 m s^{-1}. The mean SO_2 concentration was 24.7 ppb during these events. Over the entire measurement campaign however, average wind speed was considerably higher, 2.8 m s^{-1}, and the air arrived predominantly from the east. In summary, the majority of higher SO_2 events were observed in calmer conditions when the air arriving at the site had passed over nearby land; these observations provide further evidence for the influence of local sources of pollution. ~~A pollution rose is shown in Fig. 6 to show the relationship between gaseous SO_2 and wind direction. SO_2 concentrations below 5 ppb have been excluded in order to investigate the wind conditions when the spikes in SO_2 concentration occur in more detail. In the lower right corner of the plot, 'mean' represents the mean SO_2 concentration (20.1 ppbv) and 'calm' represents the fraction of data that cannot be attributed to a specific wind direction (7.1%). During~~

Formatted: Subscript
Formatted: Subscript
Formatted: Subscript
Formatted: Subscript
Formatted: Subscript
Formatted: Subscript
Formatted: Subscript
Formatted: Superscript
Formatted: Subscript
Formatted: Superscript
Formatted: Subscript

these elevated (≥ 5 ppbv) SO_2 periods, weak south westerlies dominated and the average wind speed was 1.1 m s^{-1}. A different situation was observed during the lower (< 5 ppbv) SO_2 periods; average wind speed was considerably higher, 2.8 m s^{-1}, and the air arrived predominantly from the east. In summary, the majority of higher SO_2 events were observed in calmer conditions when the air arriving at the site had passed over land to the south west of Bachok; this provides further evidence that the site is influenced by local sources of pollution.

Figure 65: Pollution rose plots to show the relationship between wind direction and SO_2 concentration (≥ 5 ppb) at the Bachok measurement site. The left panel represents recorded SO_2 concentrations ≥ 5 ppb and the right panel represents all SO_2 data recorded during the measurement period. Plot constructed using the openair package in RStudio (Carslaw and Ropkins, 2012; Carslaw, 2015).

Formatted: Subscript

At the Bachok measurement site, no obvious relationship was observed between SO_2 and particulate SO_4^{2-} concentration, or between SO_4^{2-} concentration and wind direction. This is likely to be because it takes time for SO_2 to oxidise to SO_4^{2-}, and that the SO_4^{2-} fraction of the aerosol is more heavily influenced by long-range transport of aged emissions from East Asia. To investigate this further, the backward air mass trajectories were coloured by the concentration of SO_4^{2-}, as shown in Fig. 76. (upper panel). To allow for comparison with Fig. 1, trajectories with a mean height of 80 m or below are shown on the left panel and trajectories with a mean height greater than 80 m are shown on the right panel. At the lower altitudes (≤ 80 m), it is clear that The plot clearly shows that the SO_4^{2-} content of the aerosol is highest (*ca.* 14 15 – 20 µg m^{-3}) when the site is influenced by continental air masses from industrialized regions of East Asia, and lowerst when the air masses have a more significant marine influence. This trend is less clear at higher altitudes (right panel, mean height > 80 m), but nevertheless some of the lowest SO_4^{2-} levels are observed (~ 5 µg m^{-3}) when marine air that has passed over the East and South China Sea arrives at the site. With this information availablein mind, it is useful to perform cluster analysis on the back trajectories; this type of analysis groups air masses of similar geographic origin together, which provides more information on pollutant species with similar chemical histories. A distance matrix is used to create a specified number of clusters with the most different air mass pathways. Figure Fig. 8 7 shows the 5-cluster solution to back trajectories calculated for the Bachok site during the measurement campaign.

Formatted: Subscript
Formatted: Superscript
Formatted: Superscript

Figure 76: 7-day HYSPLIT backward air mass trajectories centred on the Bachok research station between 18-01-2014 and 07-02-2014. The back trajectories are coloured by the concentration of SO_4^{2-} (µg m^{-3}). Trajectories with a mean height of 80 m or below are shown in the left panel and trajectories with a mean height greater than 80 m are shown in the right panel.Plot constructed using the openair package in RStudio (Carslaw and Ropkins, 2012; Carslaw, 2015).

Figure 87: 5-cluster solution to backward air mass trajectories centred on the Bachok research station between 18-01-2014 and 07-02-2014. Plot constructed using the openair package in RStudio (Carslaw and Ropkins, 2012; Carslaw, 2015).

Clusters 1~~2~~ and 3 were associated with mean SO_4^{2-} concentrations of 14.4 and 13.8 µg m^{-3} respectively. The mean altitude of cluster ~~2~~ 1 was ~~65~~ 72 m and the mean altitude of cluster 3 was 501 m. Full details of the air mass trajectories within each cluster are detailed in the Supplement (Table S3). These clusters contained air masses that had passed over several highly industrialised regions en route to Bachok, including cities such as ~~Zhanjiang~~ Guangzhou (China) and Ho Chi Minh City (Vietnam). Average SO_4^{2-} concentrations for clusters ~~1~~ 2 and 4 were 8.4 and 8.3 µg m^{-3}, with mean altitudes of 169 and 37 m respectively. These air masses are likely to have experienced some continental influence from the east coast of China and the island of Taiwan, but have a much more significant marine influence from passing over the South China Sea before arriving at Bachok. For air masses within cluster 1 – 4, the concentration of SO_4^{2-} increases with decreasing altitude and increasing influence from industrialised regions. The mean altitude of air masses within cluster 5 was 1027 m, *i.e.* significantly higher than air masses in clusters 1 – 4. Furthermore, the air masses in cluster 5 arriving at the site are not a result of north-easterly monsoon winds from East Asian countries travelling across the South China Sea. Instead, there is evidence of a cyclonic weather system off the coast of the island of Borneo over the South China Sea. The air masses in cluster 5 arrived during the final 24-hour period of the measurement campaign and only one SO_4^{2-} measurement is available (18.1 µg m^{-3}). It is not possible to fully understand the nature of air masses from this different region without further measurements. ~~These air masses may have experienced some continental influence from the east coast of China but mainly passed over the South China Sea before arriving at Bachok. Air masses within cluster 5 had a mean altitude of 1000 m and the SO_4^{2-} concentration was 18.1 µg m^{-3}. The air masses within this cluster came from much higher altitudes, and there is evidence of a low pressure system, generating anticlockwise winds around a possible cyclone in the South China Sea north of Borneo. Cluster 5 only incorporates the final 24-hour period of the measurement campaign (06/02/2014 12:00 – 07/02/2014 12:00) and only one SO_4^{2-} measurement is available (18.1 µg m^{-3}). Further measurements are needed under similar conditions in order to fully understand the nature of air masses from this region.~~

Despite potential differences in atmospheric lifetimes and behaviour, other pollutants aside from SO_4^{2-} can provide further~~Further~~ evidence that substantial amounts of industrial pollution from East Asia are undergoing atmospheric transport to tropical regions of the western Pacific. For example, ~~is provided in a separate study by~~ Oram et al. (2017)~~.~~ measured ~~C~~chlorine-containing very short-lived substances (Cl-VSLSs) ~~were measured~~ at the Bachok research station during the winter monsoon season in late January/ early February 2014. Cl-VSLSs are ozone depleting species with short atmospheric lifetimes, typically less than 6 months. Species include dichloromethane (CH_2Cl_2) and 1,2-dichloroethane (CH_2ClCH_2Cl). A 7-day pollution or cold-surge event was reported between 19-01-2014 and 26-01-2014, when significantly enhanced concentrations of Cl-VSLSs were observed. During this pollution episode, the measured samples were heavily impacted by emissions from the East Asian mainland, whilst this influence was less significant during the cleaner, non-polluted periods. In fact, the total median concentration of the four measured Cl-VSLSs was 546 ppt between 20 and 26 Jan, and 243 ppt during the less polluted period (27-01-2014 to 05-02-2014). Oram et al. (2017) noted that even after the cold surge event, the levels of Cl-VSLSs were

Formatted: Subscript
Formatted: Superscript
Formatted: Subscript
Formatted: Superscript
Formatted: Superscript
Formatted: Subscript
Formatted: Superscript

still significantly higher than expected, indicating that this region of the South China Sea is widely impacted by emissions from East Asia. Many other chemical pollutants, aside from short-lived chlorinated gases, will be present in these air masses from East Asia and will have a large impact on regional air quality. Oram et al. (2017) performed a Numerical Atmospheric Dispersion Modelling Environment (NAME) trajectory analysis using carbon monoxide (CO) as a tracer of industrial emissions from regions north of 20° N for 6 winter seasons (2009/2010 – 2014/2015). A strong correlation between CO and CH_2Cl_2 (a measured Cl-VSLS) was observed during the pollution episode in late January 2014. Analysis of CO time series over the 6 winter seasons revealed that cold surge events are likely to be repeated regularly each winter, demonstrating that pollution rapidly undergoes long-range transport across the South China Sea on a regular basis during the Northeast Monsoon.

3.3.3 Correlation of SO_4^{2-} with NH_4^+ and implications for aerosol acidity

Ammonium (NH_4^+) was the second most abundant ion in the aerosol; on average it made up 10.4% of the total ion content, and mean and maximum concentrations were 1.69 and 4.73 μg m^{-3} respectively. Strong positive correlation between SO_4^{2-} and NH_4^+ was observed ($R = 0.77$, $p < 0.001$). A similar observation was reported by Keywood et al. (2003) during an investigation of the sources of particles contributing to haze in the Klang Valley, Malaysia. The strong relationship between these species is due to neutralisation of SO_4^{2-} by NH_4^+. ~~It is likely that NH_3 emissions in the rural Bachok region come predominantly from agricultural practices such as animal husbandry, fertilizer use and agricultural waste burning. The measurement site is possibly influenced by other key NH_3 sources included in the Emissions Database for Global Atmospheric Research (EDGAR), such as direct soil emissions and road transport, but it is difficult to ascertain which sources are most dominant as the database does not provide local/ regional scale NH_3 emissions data for Malaysia (edgar.eu, 2016).~~Local sources of NH3 in the rural Bachok region are likely to come from agricultural practices such as animal husbandry, fertilizer use and agricultural waste burning.

The average NH_4^+/SO_4^{2-} molar ratio was 0.81, which indicated that there was insufficient gaseous NH_3 in the atmosphere to neutralise SO_4^{2-}. Under an ammonia-poor regime, the uptake of SO_4^{2-} is preferential to the uptake of NO_3^- because sulfuric acid has a lower vapour pressure than nitric acid (Seinfeld and Pandis, 2006). Although measurements of the total amounts of ammonia and sulfate in the gas, aqueous and solid phase would provide a better prediction of the aerosol acidity, the results presented in this study indicated that an ammonia-poor regime exists, and that the aerosol is likely to be acidic. In these scenarios, the NH_3 partial pressure is low, and therefore the NH_3-HNO_3 partial pressure product is also low, meaning that the concentrations of ammonium nitrate are low or zero (Seinfeld and Pandis, 2006). This hypothesis can be supported by the fact that NO_3^- concentrations in this study were very low, ranging from 0.005 to 1.52 μg m^{-3}. As a result, NO_3^- made up a significantly smaller fraction of the total ion content compared to SO_4^{2-}; average percentage mass composition of the total ion content was 3.8% for NO_3^- and 65.6% for SO_4^{2-}.

To estimate proton loading in atmospheric particles, the strong acidity approach can be used, as shown in Eq. (7). This approach assumes that any deficit in measured cation charge compared to measured anion charge can be attributed to H^+. Total anion and total cation equivalents can be estimated using Eq. (8) and Eq. (9).

$$strong\ acidity\ (\mu eq.m^{-3}) = \sum anion\ equivs.\ (\mu eq.m^{-3}) - \sum cation\ equivs.\ (\mu eq.m^{-3}) \quad (7)$$

$$\sum anion\ equivs.\ (\mu eq.m^{-3}) = \frac{SO_4^{2-}}{48} + \frac{NO_3^-}{62} + \frac{Cl^-}{35.5} + \frac{PO_4^{3-}}{31.6} + \frac{C_2O_4^{2-}}{44} + \frac{NO_2^-}{46} + \frac{CH_3SO_3^-}{95} \quad (8)$$

$$\sum cation\ equivs.\ (\mu eq.m^{-3}) = \frac{Na^+}{23} + \frac{NH_4^+}{18} + \frac{K^+}{39} + \frac{Mg^{2+}}{12} + \frac{Ca^{2+}}{20} \quad (9)$$

As shown in Fig. ~~9~~8, strong acidity values ranged from 0.03 to 0.19 µeq. m^{-3}, with an average value of 0.11 µeq. m^{-3}. The positive strong acidity values provide an initial indication that the aerosol is acidic and allows an estimate of the proton loading to be made (average H^+ = 0.11 µg m^{-3}).

Figure ~~9~~8: Predictions of particle strong acidity for the aerosol collected during the Bachok measurement campaign. Dashed lines represent predictions of maximum and minimum limits of strong acidity.~~Particle strong acidity and associated error predictions for the aerosol collected during the Bachok measurement campaign. Yellow shaded areas represent the time between sunrise and sunset (local).~~

To obtain error bars for the strong acidity predictions (Fig. ~~9~~8), H^+_{max} and H^+_{min} were calculated according to Eq. (10) and Eq. (11) respectively. For H^+_{max} the anions were adjusted up to within their uncertainties (*i.e.* +%RSD_{tot}) and the cations were adjusted down to within their uncertainties (*i.e.* -%RSD_{tot}). For H^+_{min} the anions were adjusted down and the cations were adjusted up (Murphy et al., 2017). %RSD_{tot} was estimated by combining the error of the recovery process for each ion (%RSD_{rec}, Table S1) and the error of the instrument for each ion (%RSD_{ins}, Table S2).

$$H^+_{max} = \sum max.anion\ equivalents - \sum min.\ cation\ equivalents \quad (10)$$

$$H^+_{min} = \sum min.anion\ equivalents - \sum max.cation\ equivalents \quad (11)$$

In most cases, H^+_{min} remains above zero. However, between 02-02-2014 and 06-02-2014, slightly negative H^+_{min} values between -1×10^{-3} and -2×10^{-2} µeq. m^{-3} were calculated, which are physically implausible (Murphy et al., 2017). These results highlight the possible sources of error associated with the strong acidity approach for estimating aerosol acidity. For example, Hennigan et al. (2015) report that organic acids (which are mostly excluded from this study, except for MSA and oxalic acid) can have an important influence on aerosol acidity, especially at relatively low acidities where organic acids dissociate and contribute to the ion balance. Furthermore, they can form salt complexes with inorganic species *e.g.* ammonium oxalate.

Neglecting organic acids, as well as other atmospheric species such as HCO_3^- and basic amines, will lead to inaccuracies in the calculated H^+.

Thermodynamic equilibrium models such as ISOROPPIA-II can also be used to predict aerosol pH (Fountoukis and Nenes, 2007). The ambient temperature and relative humidity data recorded nearby at the Sultan Ismail Petra airport were assumed representative of the Bachok research station, as further investigation of data from two other meteorological stations revealed that temperature and relative humidity remained consistent. A map to show the location of the three meteorological stations along the east coast, as well as the Bachok research station, can be found in the Supplement (Fig. ~~S4~~S1). The two other stations are Narathiwat airport (6.520° N, 101.743° E) and Sultan Mahmud airport (5.383° N, 103.103°E). Average relative humidity between 18-01-2014 and 07-02-2014 was 77.7% at Sultan Petra Ismail airport, 75.4% at Narathiwat airport and 77.0% at Sultan Mahmud airport. Average temperatures recorded at the stations during this time were 24.8, 25.6 and 25.4 ℃ for Sultan Petra Ismail, Sultan Mahmud and Narathiwat airport respectively.

The ISOROPPIA-II thermodynamic model predictions of $PM_{2.5}$ pH are shown in Fig. ~~10~~9. Particle pH was estimated with ISOROPPIA-II run in the reverse mode without gas phase species input, and ranged from -0.97 to 1.12 during the measurement period, implying that the aerosol was highly acidic. The pH prediction for the aerosol collected between midday on 03-02-2014 and 04-02-2014 was 7.06 and has been excluded from Fig. ~~10~~9. The particle concentrations input on this day correspond to negative values of strong acidity and therefore the model balances charge by assuming $[OH^-] > [H^+]$; this leads to a calculated pH of greater than 7. Murphy et al. (2017) have reported that pH prediction is sensitive to strong acidity in the limit of strong acidity approaching zero and that the model can be drastically improved if gas phase NH_3 and HNO_3 measurements are included. The gas-to-particle partitioning of these species is sensitive to pH under conditions commonly encountered in the atmosphere, therefore gaseous NH_3 and HNO_3 measurements provide better constraint on the thermodynamic model.

Figure ~~10~~9: Predicted $PM_{2.5}$ pH at the Bachok measurement site using ISOROPPIA-II (Fountoukis and Nenes, 2007). Dashed lines represent predictions of maximum and minimum limits of pH.~~Predicted $PM_{2.5}$ pH at the Bachok measurement site using ISOROPPIA-II. Yellow shaded areas represent the time between sunrise and sunset (local).~~

Acidic particles can have detrimental effects on human health, air quality, and the health of aquatic and terrestrial ecosystems (Hennigan et al., 2015). For example, Gwynn et al. (2000) performed a time-series analysis of acidic PM and daily mortality and morbidity in the Buffalo, New York region; several significant pollutant-health effect associations were identified, the strongest being the correlation between atmospheric SO_4^{2-} concentration and respiratory hospital admissions. Furthermore, particle acidity can influence various atmospheric chemical processes, including SO_2 oxidation, halogen chemistry, and the partitioning of ammonia, nitric acid, organic acids and isomeric epoxy diols from isoprene photooxidation (IEPOX) (Hennigan et al., 2015; Surratt et al., 2010; Lin et al., 2012). In summary, whilst some of the risks associated with aerosol acidity in

Bachok originate from local sources of pollution, it is possible that people living in these rural areas are also exposed to an additional risk, as the region appears to be sensitive to the effects of industrialisation further afield in East Asia.

3.3.4 Sources and formation of oxalate, $C_2O_4^{2-}$

Oxalic acid is the most abundant dicarboxylic acid in tropospheric aerosol (Sareen et al., 2016). This major water-soluble organic component can alter the hygroscopicity of aerosols, and can either act as cloud condensation nuclei (CCN), or reduce the surface tension of particles to form CCN (Saxena and Hildemann, 1996; Novakov and Penner, 1993; Facchini et al., 1999; Kerminen, 2001). In this study, oxalate made up 2.6% of the total measured water-soluble ion content. The average concentration was 0.42 µg m^{-3}, and throughout the measurement period the concentration ranged from 0.15 to 0.65 µg m^{-3}. Interestingly, such levels of oxalate in atmospheric aerosol are typical of urban environments, despite the fact that the Bachok research station is located in a rural coastal region. For example, Freitas et al. (2012) report average oxalate concentrations in TSP at an urban site and a rural site in Londrina City, Brazil of 0.57 and 0.03 µg m^{-3} respectively. Other reported oxalate concentrations in urban TSP include measurements of 0.10 – 0.48 µg m^{-3} in Shanghai (Jiang et al., 2011) and 0.27 µg m^{-3} in Tokyo (Sempere and Kawamura, 1994).

To investigate possible oxalate sources and formation pathways, it is necessary to consider the correlation of oxalate with different atmospheric species. Jiang et al. (2011) report using NO_2^- as an indicator for vehicle emissions, *nss*SO_4^{2-} and NO_3^- for secondary formation through different pathways, and K^+ for biomass burning. A study carried out by Huang et al. (2006) in the urban area of Shenzen (Southern China) reported that whilst good correlation of droplet oxalate with K^+ was observed (R^2 = 0.75, average diameter = 1.0 µm), there was poor correlation between oxalate and K^+ in the condensation mode (R^2 = 0.10, average diameter = 0.4 µm). This implied that whilst biomass burning was probably not an important primary source of condensation mode oxalate, it is likely that biomass burning particles act as effective CCN, promoting in-cloud sulfate and oxalate formation. In this study, *nss*K^+ levels remained below 0.7 µg m^{-3}; this likely represents background biomass burning emissions over the region during the measurement period, as evidenced by fire hotspots from satellite data shown in Fig. S4 (Giglio et al., 2003)). Strong correlation was observed between oxalate and *nss*K^+ ($R = 0.78$, $p < 0.001$) and the oxalate/*nss*K^+ ratio ranged from 0.68 to 4.64 during the Bachok measurement campaign. These ratios are significantly higher ~~suggesting that the local area was influenced by dispersed biomass burning particles rather than at the measurement site itself. However, a strong correlation was observed between oxalate and *nss*K^+ ($R = 0.78$, $p < 0.001$), and therefore the oxalate/*nss*K^+ ratio was used to predict whether biomass burning on a regional/national scale was an important primary or secondary source of oxalate. The oxalate/*nss*K^+ ratio ranged from 0.68 to 4.64 during the Bachok demonstration campaign, significantly higher~~ than those found in aerosol directly emitted from vegetation fires in the Amazon Basin (Yamasoe et al., 2000). suggesting. ~~This suggests~~ that biomass burning in the wider region influenced the secondary formation of oxalate, rather than acting as a primary source ~~of oxalate~~. A similar hypothesis was proposed by Huang and Yu (2007), who measured ambient $PM_{2.5}$ in an urban environment in the Pearl River Delta Region of China, and reported oxalate/K^+ ratios of 0.57 and 0.33 in summer and winter respectively.

Formatted: Font: Italic
Formatted: Superscript
Formatted: Font: Italic
Formatted: Superscript

It is worth noting that whilst the higher ratios reported in both studies indicate that biomass burning is not a major primary source of oxalate, measurements of oxalate and K^+ in local biomass burning aerosols (rather than aerosol in the Amazon Basin) would provide a better indication of the source contribution by biomass burning.

There was no significant correlation observed between oxalate and NO_3^-, or between oxalate and NO_2^-. The lack of correlation with NO_3^- suggests that the two species do not have similar formation pathways, and that vehicle emissions are not an important secondary source of oxalate. It is also unlikely that vehicle emissions contribute to the primary sources of oxalate, due to the lack of correlation between oxalate and NO_2^-. However, NO_2^- was only detected in 7 out of the 30 samples collected, so it is difficult to ascertain whether there is a relationship between these two species or not. Strong correlation between oxalate and *nss*SO_4^{2-} ($R = 0.69$, $p < 0.001$) was observed, suggesting a common formation pathway of the two species. It is well known that SO_4^{2-} forms *via* aqueous oxidation (Seinfeld and Pandis, 2006), and modelling studies also suggest that aqueous chemistry is a large contributor of oxalate formation globally (Myriokefalitakis et al., 2011). Furthermore, Carlton et al. (2006) report that whilst there are likely to be many sources of oxalate, oxidation of pyruvate in the aqueous phase is known to form oxalate at dilute (cloud-relevant) concentrations. Tan et al. (2012) also state that aqueous acetate oxidation is a key source of oxalate. A positive correlation between oxalate and NH_4^+ was also observed ($R = 0.73$, $p < 0.001$). A similar observation was reported by Jiang et al. (2011) in a study of aerosol oxalate in Shanghai. Using size distribution data, they were able to propose that the correlation was due to the presence of ammonium oxalate in the aerosol. In this study there is no size distribution data available, and so it is important to consider the fact that the correlation may be linked to the influence of sulfate on both NH_4^+ and oxalate in aerosol; NH_4^+ partitions to the aerosol from gaseous NH_3 in an attempt to neutralise acidic sulfate particles, whilst oxalate exhibits similar formation pathways to SO_4^{2-}.

3.3.5 Sea salt aerosol and factors affecting chloride depletion

On average, Na^+ and Cl^- contributed 7.0% and 4.1% to the total measured water-soluble ion content respectively, and 72% of the measured Na^+ was attributed to *ss*Na^+. The concentration of *ss*Na^+ ranged from 0.24 to 2.35 μg m^{-3}, whilst the concentration of Cl^- ranged from 0.003 to 2.38 μg m^{-3}. There was no correlation between *nss*Na^+ and Cl^- ($R = -0.01$), but a strong positive correlation between *ss*Na^+ and Cl^- was observed ($R = 0.84$, $p < 0.001$). During the measurement period, the $Cl^-/ssNa^+$ molar ratio ranged from 0.003 to 1.10 with an average value of 0.40. A time series of $Cl^-/ssNa^+$ molar ratio can be found in the Supplement (Fig. S5). Significant Cl^- depletion was observed, as all of the ratios recorded were lower than that of bulk seawater, 1.18 (Boreddy and Kawamura, 2015). ~~Figure~~ Fig.~~11~~ 10 shows backward air mass trajectories arriving at the Bachok research station, coloured by the $Cl^-/ssNa^+$ molar ratio.

Figure ~~11~~10: 7-day HYSPLIT back trajectories centred on the Bachok research station, between 18-01-2014 and 07-02-2014. The back trajectories are coloured by the $Cl^-/ssNa^+$ molar ratio. Trajectories with a mean height of 80 m or below are shown in the left

panel and trajectories with a mean height greater than 80 m are shown in the right panel. ~~Plot constructed using the openair package in RStudio (Carslaw and Ropkins, 2012; Carslaw, 2015).~~

A study of marine aerosol at remote Chichijima Island in the western North Pacific during 2001 and 2002 reported that mean Cl^-/Na^+ molar ratios were highest (1.34) in September 2001 and lowest (0.30) in May 2002, and the mean ratio across the 2-year period was 1.10 (Boreddy et al., 2014). Boreddy et al. (2014) reported that the observed chloride depletion was likely due to acid displacement occurring as a result of atmospheric mixing of anthropogenic pollutants such as SO_x and NO_x. Acid displacement can occur when sea salt particles react with acids such as H_2SO_4, HNO_3, oxalic acid ($C_2H_2O_4$) and methanesulfonic acid (CH_3SO_3H) in the atmosphere. Such processes are of atmospheric importance as they lead to the formation of gaseous HCl and potentially affect acid deposition conditions in the region. It is widely accepted that Cl^- depletion through the volatilization of HCl *via* acid displacement occurs particularly in polluted marine air masses (Newberg et al., 2005; Sturges and Shaw, 1993). In this study, the lowest $Cl^-/ssNa^+$ ratios were observed when air masses arriving at the site had previously passed over highly industrialised countries such as China and Vietnam (~~Figure~~ Fig. ~~11~~10). Higher $Cl^-/ssNa^+$ ratios are found ~~when in the~~ marine air masses ~~are~~ from less polluted regions. It is possible that aerosol, particularly in northern China, may be rich in chloride in the winter due to coal burning. However, this study suggests that the influence of other anthropogenic pollutants, such as HNO_3 and H_2SO_4, means that as the air is transported over the South China Sea to the Bachok region, significant Cl^- depletion can occur prior to arrival at the measurement site. In a more recent study, Boreddy and Kawamura performed regression analysis between the Cl^-/Na^+ mass ratio and various acidic species, including $nssSO_4^{2-}$, NO_3^-, MSA^- and oxalic acid. They found a moderate negative correlation between Cl^-/Na^+ mass ratio and $nssSO_4^{2-}$, and a moderate to weak negative correlation with NO_3^-; this suggested that sulfate had a higher influence on chloride depletion than nitrate. Furthermore, whilst MSA^- moderately correlated with the Cl^-/Na^+ mass ratio in the summer, there was significant negative correlation between oxalic acid and the mass ratio in the other three seasons, providing confirmation that oxalic acid plays an important role in chloride loss at Chichijima Island. A similar regression analysis was carried out on the measurements obtained during the Bachok measurement campaign, and whilst a weak negative correlation was found between SO_4^{2-} and the $Cl^-/ssNa^+$ mass ratio ($R = -0.41$, $p < 0.001$), there was no correlation of the $Cl^-/ssNa^+$ mass ratio with oxalate or MSA^-. These results imply that whilst H_2SO_4 played an important role in chloride depletion, methanesulfonic acid and oxalic acid may not have done. Interestingly, a strong positive correlation was observed between NO_3^- and $Cl^-/ssNa^+$ mass ratio ($R = 0.82$, $p < 0.001$). These measurements may be linked to each other through the important role of H_2SO_4 in the atmosphere. Acid displacement, when sea salt reacts with H_2SO_4, leads to the removal of Cl^- from the aerosol as gaseous HCl, and a partitioning of SO_4^{2-} to the aerosol as Na_2SO_4. Furthermore, under an ammonia-poor regime (as observed in this study), H_2SO_4 has a lower vapour pressure than HNO_3, leading to the preferential formation of ammonium sulfate over ammonium nitrate when there is insufficient NH_3 available to fully neutralize sulfate and nitrate (Seinfeld and Pandis, 2006).

3.3.6 Using *nss*Ca^{2+} as a potential tracer for dust episodes

NssCa^{2+} can be used as a tracer for atmospheric dust (Boreddy and Kawamura, 2015). The average concentration of *nss*Ca^{2+} during the measurement campaign was 0.07 µg m^{-3} and the maximum concentration recorded was 0.28 µg m^{-3}. On most days, the *nss*Ca^{2+} concentration was below 0.10 µg m^{-3}, but between midday on 30-01-2014 and midnight on 31-01-2014 (local times), elevated *nss*Ca^{2+} levels were observed and the average concentration during this period was 0.22 µg m^{-3}. The same trend was observed for PO_4^{3-}; the average concentration across the entire measurement period was 0.34 µg m^{-3}, but during this 12-hour episode the PO_4^{3-} concentration increased to 1.88 µg m^{-3}. The increase in ion concentration was less pronounced for *nss*Na^+ and Mg^{2+}, but the concentrations were still 0.26 and 0.88 µg m^{-3} above the average for the whole measurement period respectively. Time series plots for *nss*Ca^{2+}, PO_4^{3-}, Mg^{2+} and *nss*Na^+ can be found in the Supplement (~~Figure~~ Fig. S6).

Between midday on 30-01-2014 and midnight on 31-01-2014, *nss*Ca^{2+} contributed significantly (1.26%) to the total measured water-soluble ion content compared to the average contribution during the remainder of the measurement period (0.35%). The Bachok research station is located in the outflow region of Asian dusts, and these measurements suggest that long-range transport of Asian dusts over the measurement site has occurred during this time. In fact, during this episode, the back trajectories arriving at the site can be traced back to the North China Plains and the Horqin Sandy Land in East China; source attribution studies by Ginoux et al. (2012) have revealed that large anthropogenic dust sources are found in these regions. In the future, it is important that longer term measurements are carried out at the Bachok research station, to provide confirmation that dust episodes in these regions of Asia are responsible for the elevated levels of *nss*Ca^{2+} and other associated ions. Dust is one of the most abundant types of aerosol in the atmosphere and can have important impacts on both air quality and climate, therefore it is important that seasonal and annual trends in water-soluble ions are studied in more detail at the Bachok research station.

4 Conclusions

An accurate and reliable technique relying on ion chromatography has been used to make time-resolved measurements of water-soluble ions in atmospheric aerosol at the Bachok Marine and Atmospheric research station. Using meteorological data from the nearby airport, and HYSPLIT backward air mass trajectories centred on the Bachok research station, it was possible to observe both the diurnal wind pattern behaviour, and assess where the air masses arriving at the site originated from. Air quality at this remote location is influenced by local anthropogenic and biogenic emissions, as well as marine air masses from the South China Sea and aged emissions transported from highly polluted East Asian regions during the winter monsoon season. In general, the site was influenced by south westerlies coming from the land from the early hours of the morning until approximately 11 am, and then a dramatic shift in wind direction occurred and a sea breeze was present for the remainder of the day. This shift was accompanied by a drop in the concentrations of NO_x and anthropogenic VOCs (Dunmore et al., 2016).

Twelve atmospheric water-soluble ions were measured in this study and SO_4^{2-} was found to be the most dominant ion present, making up 66% of the total measured ion content on average. The non-sea salt and sea salt components of SO_4^{2-}, Na^+, K^+ and Ca^{2+} were determined, and it was found that 96% of the measured SO_4^{2-} was non-sea salt SO_4^{2-}. Predictions of aerosol pH were made using the ISOROPPIA-II thermodynamic model and it was estimated that the aerosol was highly acidic, with pH values ranging from -0.97 to 1.12; such levels of acidity are likely to have a detrimental impact on human health and the health of ecosystems at this remote coastal location. A clear difference in aerosol composition was found between continental air masses originating from industrialised regions of East Asia and marine air masses predominantly influenced by the South China Sea. For example, elevated SO_4^{2-} concentrations were observed when continental air masses that had passed over highly industrialised regions of East Asia arrived at the measurement site.

Correlation analyses amongst ionic species and assessment of ratios between different ions provided an insight into common sources and formation pathways of key atmospheric ions. Oxalate concentrations were recorded and found to be more comparable to measurements made at urban locations rather than rural ones. A strong correlation of $C_2O_4^{2-}$ with SO_4^{2-} suggested a common aqueous oxidation formation pathway. Strong correlation between $C_2O_4^{2-}$ and K^+ coupled with high $C_2O_4^{2-}/nssK^+$ ratios indicated that biomass burning was an important secondary source of oxalate in the Bachok region, whereas lack of correlation with NO_2^- and NO_3^- suggested that vehicular emissions were not an important source. The average $Cl^-/ssNa^+$ molar ratio during the measurement campaign was 0.40, significantly lower than that of bulk seawater (1.18). Analysis of back trajectories revealed that chloride depletion was greater when the aerosol was more influenced by anthropogenic sources of pollution. Elevated levels of $nssCa^{2+}$ and other ions such as PO_4^{3-}, Mg^{2+} and $nssNa^+$ were observed between midday on 30-01-2014 and midnight on 31-01-2014. Assuming that $nssCa^{2+}$ can be used as a tracer for atmospheric dust, it was proposed that the increased concentrations were a result of air masses arriving at the site from the North China Plains and Horqin Sandy Lands. Longer term measurements are required to fully investigate the influence of Asian dusts at this remote coastal location.

To our knowledge, time-resolved measurements of water-soluble ions in $PM_{2.5}$ are virtually non-existent in rural locations on the east coast of Peninsular Malaysia. The data presented in this study has demonstrated the capabilities of the new atmospheric tower at the Bachok research station and has provided an initial insight into factors affecting aerosol composition on this coastline. In the future, it is important that longer term measurements are carried out, with increased time-resolved sampling and particle size fractionation, to provide a better understanding of the factors affecting aerosol composition at this measurement site. This remote location is susceptible to the effects of local, regional and international air pollution, and rapid industrialisation in East Asia is influencing air quality along the east coast of Peninsular Malaysia.

Data availability. Raw data is available on PURE (DOI: 10.15124/bd4a9045-832b-4ff8-aecc-ef1653603f1d).

Author contribution. All authors contributed to the final version of this article. Naomi J Farren analysed the aerosol samples and wrote the paper under the supervision of Jacqueline F Hamilton. Rachel E Dunmore collected the aerosol samples. M Iqbal Mead, Mohd Shahrul Mohd Nadzir, Azizan Abu Samah and Siew-Moi Phang coordinate and manage the University of Malaya BMRS. William T Sturges coordinated the Bachok demonstration 'International Opportunities Fund' campaign.

Competing interests. The authors declare that they have no conflict of interest.

Acknowledgements. The financial support of the Natural Environment Research Council (N. Farren, PhD studentship NE/L501751/1) is gratefully acknowledged. N. Farren would like to thank David Carslaw for his assistance using Openair. All authors would like to acknowledge NERC (NE/J016012/1 and NE/J016047/1) for funding the Bachok demonstration 'International Opportunities Fund' campaign and HICoE-MoHE IOES-2014 (Air-Ocean-Land Interactions) for supporting the Bachok Marine Research Station facilities.

References

Ashfold, M. J., Latif, M. T., Samah, A. A., Mead, M. I., and Harris, N. R. P.: Influence of Northeast Monsoon cold surges on air quality in Southeast Asia, Atmos. Environ., 166, 498-509, 10.1016/j.atmosenv.2017.07.047, 2017.

Behrenfeld, M. J., O'Malley, R. T., Siegel, D. A., McClain, C. R., Sarmiento, J. L., Feldman, G. C., Milligan, A. J., Falkowski, P. G., Letelier, R. M., and Boss, E. S.: Climate-driven trends in contemporary ocean productivity, Nature, 444, 752-755, 10.1038/nature05317, 2006.

Bloss, W. J., Evans, M. J., Lee, J. D., Sommariva, R., Heard, D. E., and Pilling, M. J.: The oxidative capacity of the troposphere: Coupling of field measurements of OH and a global chemistry transport model, Faraday Discuss, 130, 425-436, 10.1039/b419090d, 2005.

Boreddy, S. K. R., Kawamura, K., and Jung, J. S.: Hygroscopic properties of particles nebulized from water extracts of aerosols collected at Chichijima Island in the western North Pacific: An outflow region of Asian dust, J Geophys Res-Atmos, 119, 167-178, 10.1002/2013JD020626, 2014.

Boreddy, S. K. R., and Kawamura, K.: A 12-year observation of water-soluble ions in TSP aerosols collected at a remote marine location in the western North Pacific: an outflow region of Asian dust, Atmos Chem Phys, 15, 6437-6453, 10.5194/acp-15-6437-2015, 2015.

Bowen, H. J. M.: Environmental chemistry of the elements, Academic Press, London, 1979.

Carlton, A. G., Turpin, B. J., Lim, H. J., Altieri, K. E., and Seitzinger, S.: Link between isoprene and secondary organic aerosol (SOA): Pyruvic acid oxidation yields low volatility organic acids in clouds, Geophys Res Lett, 33, Artn L06822

10.1029/2005gl025374, 2006.

Carpenter, L. J., Fleming, Z. L., Read, K. A., Lee, J. D., Moller, S. J., Hopkins, J. R., Purvis, R. M., Lewis, A. C., Muller, K., Heinold, B., Herrmann, H., Fomba, K. W., van Pinxteren, D., Muller, C., Tegen, I., Wiedensohler, A., Muller, T., Niedermeier, N., Achterberg, E. P., Patey, M. D., Kozlova, E. A., Heimann, M., Heard, D. E., Plane, J. M. C., Mahajan, A., Oetjen, H., Ingham, T., Stone, D., Whalley, L. K., Evans, M. J., Pilling, M. J., Leigh, R. J., Monks, P. S., Karunaharan, A., Vaughan, S., Arnold, S. R., Tschritter, J., Pohler, D., Friess, U., Holla, R., Mendes, L. M., Lopez, H., Faria, B., Manning, A. J., and Wallace, D. W. R.: Seasonal characteristics of tropical marine boundary layer air measured at the Cape Verde Atmospheric Observatory, J Atmos Chem, 67, 87-140, 10.1007/s10874-011-9206-1, 2010.

Carslaw, D. C., and Ropkins, K.: openair - An R package for air quality data analysis, Environ Modell Softw, 27-28, 52-61, 10.1016/j.envsoft.2011.09.008, 2012.

Carslaw, D. C.: The openair manual - open-source tools for analysing air pollution data. Manual for version 1.1-4., King's College London, 2015.

Charlson, R. J., Langner, J., Rodhe, H., Leovy, C. B., and Warren, S. G.: Perturbation of the Northern-Hemisphere Radiative Balance by Backscattering from Anthropogenic Sulfate Aerosols, Tellus A, 43, 152-163, DOI 10.1034/j.1600-0870.1991.00013.x, 1991.

Dominick, D., Latif, M. T., Juneng, L., Khan, M. F., Amil, N., Mead, M. I., Nadzir, M. S. M., Moi, P. S., Abu Samah, A., Ashfold, M. J., Sturges, W. T., Harris, N. R. P., Robinson, A. D., and Pyle, J. A.: Characterisation of particle mass and number concentration on the east coast of the Malaysian Peninsula during the northeast monsoon, Atmos. Environ., 117, 187-199, 10.1016/j.atmosenv.2015.07.018, 2015.

Draxler, R. R., and Hess, G. D.: Description of the HYSPLIT_4 modeling system, NOAA Air Resources Laboratory, Silver Spring, MD, NOAA Tech. Memo. ERL ARL-224, 24, 1997.

Draxler, R. R., and Hess, G. D.: An overview of the HYSPLIT_4 modeling system of trajectories, dispersion, and deposition, Aust. Meteor. Mag., 47, 295-308, 1998.

Draxler, R. R.: HYSPLIT4 user's guide, NOAA Air Resources Laboratory, Silver Spring, MD, NOAA Tech. Memo. ERL ARL-230, 1999.

Dunmore, R. E., Hopkins, J. R., Lidster, R. T., Mead, M. I., Bandy, B. J., Forster, G., Oram, D. E., Sturges, W. T., Phang, S. M., Abu Samah, A., and Hamilton, J. F.: Development of a Combined Heart-Cut and Comprehensive Two-Dimensional Gas Chromatography System to Extend the Carbon Range of Volatile Organic Compounds Analysis in a Single Instrument, Separations, 3, ARTN 21

10.3390/separations3030021, 2016.

EPA, Title 40 Protection of Environment Part 136 Guidelines Establishing Test Procedures for the Analysis of Pollutants. In *Electronic Code of Federal Regulations* [Online] U.S. Government Publishing Office: Washington, DC, 2017. https://www.ecfr.gov/cgi-bin/text-

idx?SID=57d5771415f8a36cb8c0e2ca2a1583a2&mc=true&node=pt40.25.136&rgn=div5#ap40.25.136_17.b (accessed 20-07-2017).

Facchini, M. C., Mircea, M., Fuzzi, S., and Charlson, R. J.: Cloud albedo enhancement by surface-active organic solutes in growing droplets, Nature, 401, 257-259, Doi 10.1038/45758, 1999.

Fisher, J. A., Jacob, D. J., Wang, Q. Q., Bahreini, R., Carouge, C. C., Cubison, M. J., Dibb, J. E., Diehl, T., Jimenez, J. L., Leibensperger, E. M., Lu, Z. F., Meinders, M. B. J., Pye, H. O. T., Quinn, P. K., Sharma, S., Streets, D. G., van Donkelaar, A., and Yantosca, R. M.: Sources, distribution, and acidity of sulfate-ammonium aerosol in the Arctic in winter-spring, Atmos. Environ., 45, 7301-7318, 10.1016/j.atmosenv.2011.08.030, 2011.

Fountoukis, C., and Nenes, A.: ISORROPIA II: a computationally efficient thermodynamic equilibrium model for K+-Ca2+-Mg2+-Nh(4)(+)-Na+-SO42--NO3--Cl--H2O aerosols, Atmos Chem Phys, 7, 4639-4659, 2007.

Freitas, A. D., Martins, L. D., and Solci, M. C.: Size-Segregated Particulate Matter and Carboxylic Acids over Urban and Rural Sites in Londrina City, Brazil, J Brazil Chem Soc, 23, 921-930, 2012.

Garreaud, R. D.: Subtropical cold surges: Regional aspects and global distribution, Int J Climatol, 21, 1181-1197, Doi 10.1002/Joc.687, 2001.

Global Atmospheric Watch Station Information System (GAWSIS): https://gawsis.meteoswiss.ch/GAWSIS//index.html#/, access: 12-04-2017, 2017.

Giglio, L., Descloitres, J., Justice, C. O., and Kaufman, Y. J.: An enhanced contextual fire detection algorithm for MODIS, Remote Sens Environ, 87, 273-282, 10.1016/S0034-4257(03)00184-6, 2003.

Ginoux, P., Prospero, J. M., Gill, T. E., Hsu, N. C., and Zhao, M.: Global-Scale Attribution of Anthropogenic and Natural Dust Sources and Their Emission Rates Based on Modis Deep Blue Aerosol Products, Rev Geophys, 50, Artn Rg3005

10.1029/2012rg000388, 2012.

Gwynn, R. C., Burnett, R. T., and Thurston, G. D.: A time-series analysis of acidic particulate matter and daily mortality and morbidity in the Buffalo, New York, region, Environ Health Persp, 108, 125-133, Doi 10.2307/3454510, 2000.

Hennigan, C. J., Izumi, J., Sullivan, A. P., Weber, R. J., and Nenes, A.: A critical evaluation of proxy methods used to estimate the acidity of atmospheric particles, Atmos Chem Phys, 15, 2775-2790, 10.5194/acp-15-2775-2015, 2015.

Huang, X. F., Yu, J. Z., He, L. Y., and Yuan, Z. B.: Water-soluble organic carbon and oxalate in aerosols at a coastal urban site in China: Size distribution characteristics, sources, and formation mechanisms, J Geophys Res-Atmos, 111, Artn D22212

10.1029/2006jd007408, 2006.

Huang, X. F., and Yu, J. Z.: Is vehicle exhaust a significant primary source of oxalic acid in ambient aerosols?, Geophys Res Lett, 34, Artn L02808

10.1029/2006gl028457, 2007.

Ismail, M., Yuen, F. S., and Abdullah, S. S.: Particulate Matter Status and its Relationship with Meteorological Factors in the East Coast of Peninsular Malaysia, Journal of Engineering and Applied Sciences, 11, 2588-2593, 2016.

Jiang, Y., Zhuang, G., Wang, Q., Liu, T., Huang, K., Fu, J. S., Li, J., Lin, Y., Zhang, R., and Deng, C.: Characteristics, sources and formation of aerosol oxalate in an Eastern Asia megacity and its implication to haze pollution, Atmos Chem Phys Discuss, 11, 22075-22112, 10.5194/acpd-11-22075-2011, 2011.

Kerminen, V. M.: Relative roles of secondary sulfate and organics in atmospheric cloud condensation nuclei production, J Geophys Res-Atmos, 106, 17321-17333, Doi 10.1029/2001jd900204, 2001.

Keywood, M. D., Ayers, G. P., Gras, J. L., Boers, R., and Leong, C. P.: Haze in the Klang Valley of Malaysia, Atmos Chem Phys, 3, 591-605, 2003.

Lawrence, M. G., Jockel, P., and von Kuhlmann, R.: What does the global mean OH concentration tell us?, Atmos Chem Phys, 1, 37-49, 2001.

Legrand, M., and Pasteur, E. C.: Methane sulfonic acid to non-sea-salt sulfate ratio in coastal Antarctic aerosol and surface snow, J Geophys Res-Atmos, 103, 10991-11006, Doi 10.1029/98jd00929, 1998.

Lin, Y. H., Zhang, Z. F., Docherty, K. S., Zhang, H. F., Budisulistiorini, S. H., Rubitschun, C. L., Shaw, S. L., Knipping, E. M., Edgerton, E. S., Kleindienst, T. E., Gold, A., and Surratt, J. D.: Isoprene Epoxydiols as Precursors to Secondary Organic Aerosol Formation: Acid-Catalyzed Reactive Uptake Studies with Authentic Compounds, Environ. Sci. Technol., 46, 250-258, 10.1021/es202554c, 2012.

Murphy, J. G., Gregoire, P. K., Tevlin, A. G., Wentworth, G. R., Ellis, R. A., Markovic, M. Z., and Vandenboer, T. C.: Observational constraints on particle acidity using measurements and modelling of particles and gases, Faraday Discuss, xx, 1-17, 2017.

Myriokefalitakis, S., Tsigaridis, K., Mihalopoulos, N., Sciare, J., Nenes, A., Kawamura, K., Segers, A., and Kanakidou, M.: In-cloud oxalate formation in the global troposphere: a 3-D modeling study, Atmos Chem Phys, 11, 5761-5782, 10.5194/acp-11-5761-2011, 2011.

Neale, R., and Slingo, J.: The maritime continent and its role in the global climate: A GCM study, J Climate, 16, 834-848, Doi 10.1175/1520-0442(2003)016<0834:Tmcair>2.0.Co;2, 2003.

Newberg, J. T., Matthew, B. M., and Anastasio, C.: Chloride and bromide depletions in sea-salt particles over the northeastern Pacific Ocean, J Geophys Res-Atmos, 110, Artn D06209

10.1029/2004jd005446, 2005.

National Oceanic and Atmospheric Administration Integrated Surface Database https://www.ncdc.noaa.gov/isd, access: 20-07-2017, 2003.

Novakov, T., and Penner, J. E.: Large Contribution of Organic Aerosols to Cloud-Condensation-Nuclei Concentrations, Nature, 365, 823-826, Doi 10.1038/365823a0, 1993.

Oram, D. E., Ashfold, M. J., Laube, J. C., Gooch, L. J., Humphrey, S., Sturges, W. T., Leedham-Elvidge, E., Forster, G. L., Harris, N. R. P., Mead, M. I., Abu Samah, A., Phang, S. M., Ou-Yang, C. F., Lin, N. H., Wang, J. L., Baker, A. K., Brenninkmeijer, C. A. M., and Sherry, D.: A growing threat to the ozone layer from short-lived anthropogenic chlorocarbons, Atmos Chem Phys, 17, 11929-11941, 10.5194/acp-17-11929-2017, 2017.

Pyle, J. A., Ashfold, M. J., Harris, N. R. P., Robinson, A. D., Warwick, N. J., Carver, G. D., Gostlow, B., O'Brien, L. M., Manning, A. J., Phang, S. M., Yong, S. E., Leong, K. P., Ung, E. H., and Ong, S.: Bromoform in the tropical boundary layer of the Maritime Continent during OP3, Atmos Chem Phys, 11, 529-542, 10.5194/acp-11-529-2011, 2011.

Ripp, J.: Analytical Detection Limit Guidance and Laboratory Guide for Determining Method Detection Limits, Wisconsin Department of Natural Resources, Madison, WI, PUBL-TS-056-96, 1996.

Robinson, A. D., Harris, N. R. P., Ashfold, M. J., Gostlow, B., Warwick, N. J., O'Brien, L. M., Beardmore, E. J., Nadzir, M. S. M., Phang, S. M., Samah, A. A., Ong, S., Ung, H. E., Peng, L. K., Yong, S. E., Mohamad, M., and Pyle, J. A.: Long-term halocarbon observations from a coastal and an inland site in Sabah, Malaysian Borneo, Atmos Chem Phys, 14, 8369-8388, 10.5194/acp-14-8369-2014, 2014.

Sareen, N., Carlton, A. G., Surratt, J. D., Gold, A., Lee, B., Lopez-Hilfiker, F. D., Mohr, C., Thornton, J. A., Zhang, Z. F., Lim, Y. B., and Turpin, B. J.: Identifying precursors and aqueous organic aerosol formation pathways during the SOAS campaign, Atmos Chem Phys, 16, 14409-14420, 10.5194/acp-16-14409-2016, 2016.

Savoie, D. L., and Prospero, J. M.: Comparison of Oceanic and Continental Sources of Non-Sea-Salt Sulfate over the Pacific-Ocean, Nature, 339, 685-687, Doi 10.1038/339685a0, 1989.

Saxena, P., and Hildemann, L. M.: Water-soluble organics in atmospheric particles: A critical review of the literature and application of thermodynamics to identify candidate compounds, J Atmos Chem, 24, 57-109, Doi 10.1007/Bf00053823, 1996.

Seinfeld, J. H., and Pandis, S. N.: Atmospheric chemistry and physics : from air pollution to climate change, 2nd ed., J. Wiley, Hoboken, N.J., 1-1203 pp., 2006.

Sempere, R., and Kawamura, K.: Comparative Distributions of Dicarboxylic-Acids and Related Polar Compounds in Snow Rain and Aerosols from Urban Atmosphere, Atmos. Environ., 28, 449-459, Doi 10.1016/1352-2310(94)90123-6, 1994.

Stein, A. F., Draxler, R. R., Rolph, G. D., Stunder, B. J. B., Cohen, M. D., and Ngan, F.: Noaa's Hysplit Atmospheric Transport and Dispersion Modeling System, Bulletin of the American Meteorological Society, 96, 2059-2077, 10.1175/Bams-D-14-00110.1, 2015.

Sturges, W. T., and Shaw, G. E.: Halogens in Aerosols in Central Alaska, Atmos Environ a-Gen, 27, 2969-2977, Doi 10.1016/0960-1686(93)90329-W, 1993.

Surratt, J. D., Chan, A. W. H., Eddingsaas, N. C., Chan, M. N., Loza, C. L., Kwan, A. J., Hersey, S. P., Flagan, R. C., Wennberg, P. O., and Seinfeld, J. H.: Reactive intermediates revealed in secondary organic aerosol formation from isoprene, PNAS, 107, 6640-6645, 10.1073/pnas.0911114107, 2010.

Tahir, N. M., Suratman, S., Fong, F. T., Hamzah, M. S., and Latif, M. T.: Temporal Distribution and Chemical Characterization of Atmospheric Particulate Matter in the Eastern Coast of Peninsular Malaysia, Aerosol Air Qual Res, 13, 584-595, 10.4209/aaqr.2012.08.0216, 2013.

Tan, Y., Lim, Y. B., Altieri, K. E., Seitzinger, S. P., and Turpin, B. J.: Mechanisms leading to oligomers and SOA through aqueous photooxidation: insights from OH radical oxidation of acetic acid and methylglyoxal, Atmos Chem Phys, 12, 801-813, 10.5194/acp-12-801-2012, 2012.

Yamasoe, M. A., Artaxo, P., Miguel, A. H., and Allen, A. G.: Chemical composition of aerosol particles from direct emissions of vegetation fires in the Amazon Basin: water-soluble species and trace elements, Atmos. Environ., 34, 1641-1653, Doi 10.1016/S1352-2310(99)00329-5, 2000.

Zhang, Y., Sperber, K. R., and Boyle, J. S.: Climatology and interannual variation of the East Asian winter monsoon: Results from the 1979-95 NCEP/NCAR reanalysis, Mon Weather Rev, 125, 2605-2619, Doi 10.1175/1520-0493(1997)125<2605:Caivot>2.0.Co;2, 1997.

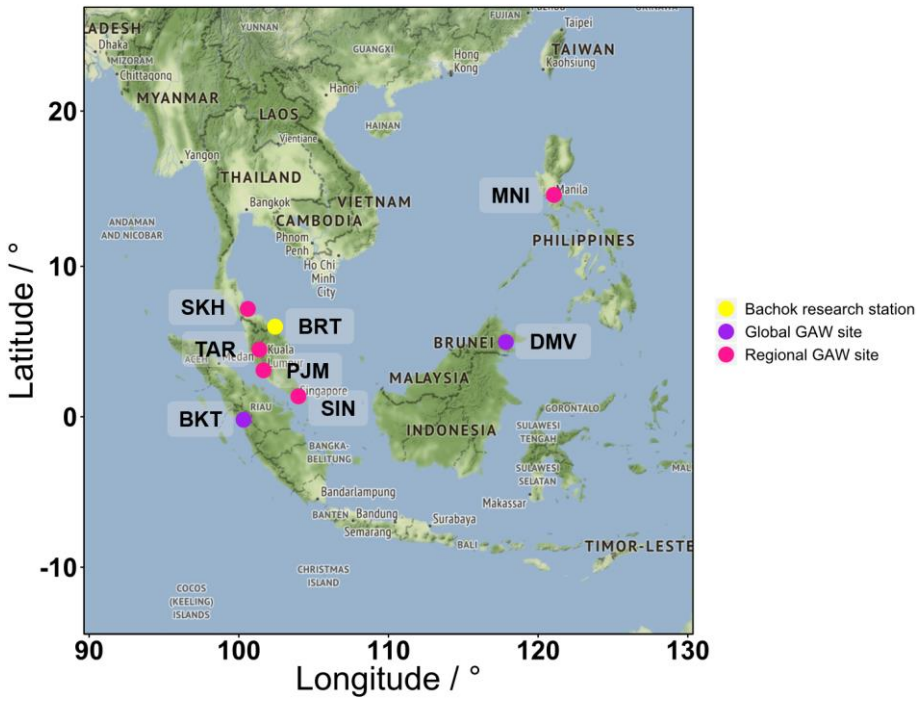

875 **Figure 1: Location of the Bachok research station (BRT) and the global ~~(green pins)~~ and regional (blue pins) GAW sites in the Maritime Continent; Danum Valley in Malaysia (DMV), Bukit Kototabang in Indonesia (BKT), Manila in Philippines (MNI), Songkhla in Thailand (SKH), Tanah Rata in Malaysia (TAR), Petaling Jaya in Malaysia (PJM) and Singapore (SIN) (gawsis.ch, 2017). ~~The red pin shows the location of the Bachok Marine and Atmospheric Research Station. Map created using google maps (google.com, 2017).~~**

880

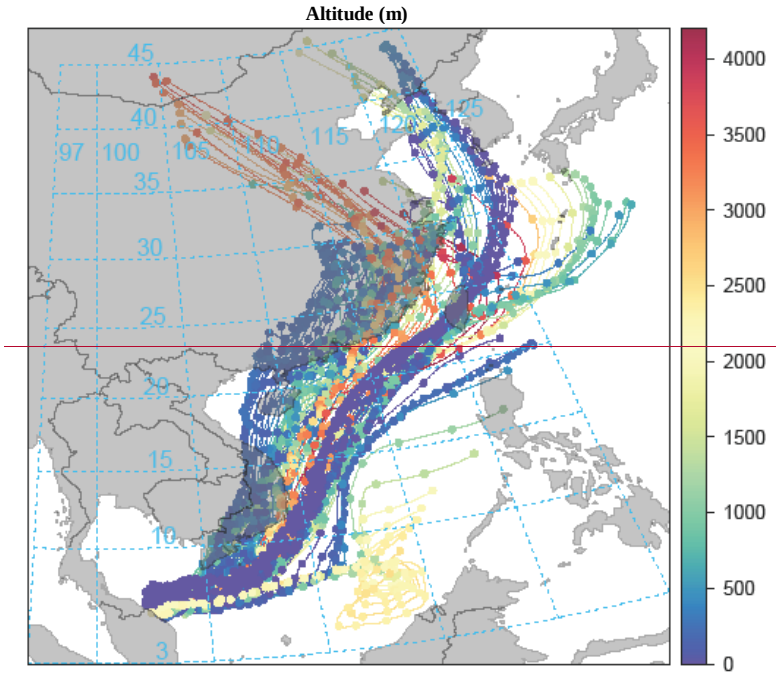
Altitude (m)
45
40
97
100
105
110
115
120
125
35
30
25
20
15
10
3
4000
3500
3000
2500
2000
1500
1000
500
0

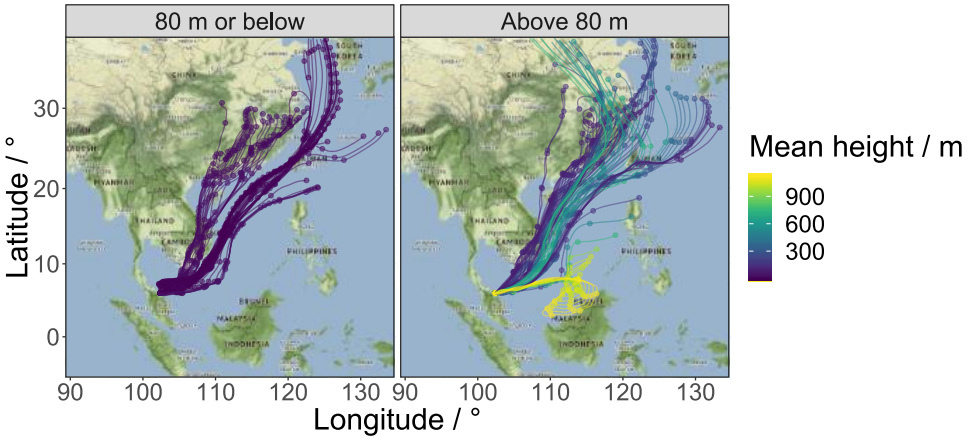

Figure 2: 7-day HYSPLIT backward air mass trajectories centred on the Bachok Marine and Atmospheric Research Station between 18-01-2014 and 07-02-2014. ~~The back trajectories~~Each trajectory is ~~are~~ coloured by the mean altitude ~~of the air mass~~ (m). Trajectories with a mean height of 80 m or below are shown in the left panel and trajectories with a mean height greater than 80 m are shown in the right panel.~~Plot constructed using the openair package in RStudio (Carslaw and Ropkins, 2012; Carslaw, 2015).~~

Formatted: Caption, Line spacing: 1.5 lines

Formatted: Justified

Formatted: Normal

Table 1: Mean and maximum ion concentrations measured throughout the measurement period. The average % mass contribution of each ion to the total measured ions is included, as well as the % of samples in which each target ion is found (%Qt).

Ion	Mean [ion] / µg m^{-3}	Maximum [ion] / µg m^{-3}	Mean % mass of total measured ion content	%Qt[a]	%RSD$_{total}$[b]
SO_4^{2-}	10.7	20.8	65.6	100	11.2
NH_4^+	1.69	4.73	10.4	100	6.38
Na^+	1.13	2.60	6.95	100	6.88
Cl^-	0.67	2.38	4.14	100	8.49
NO_3^-	0.61	1.52	3.76	100	22.6
$C_2O_4^{2-}$	0.42	0.65	2.57	97	13.9
PO_4^{3-}	0.36	2.34	2.22	93	15.4
K^+	0.38	0.67	0.67	100	6.35
Ca^{2+}	0.10	0.35	0.64	100	9.26
Mg^{2+}	0.10	0.21	0.61	100	6.72
$CH_3SO_3^-$	0.08	0.22	0.47	67	10.6
NO_2^-	0.05	0.16	0.33	23	14.3
Total	**16.2**	**27.0**	--	--	--

[a]Percentage of samples in which the target ion was above the LOQ. [b]Total error associated with each ion.

900

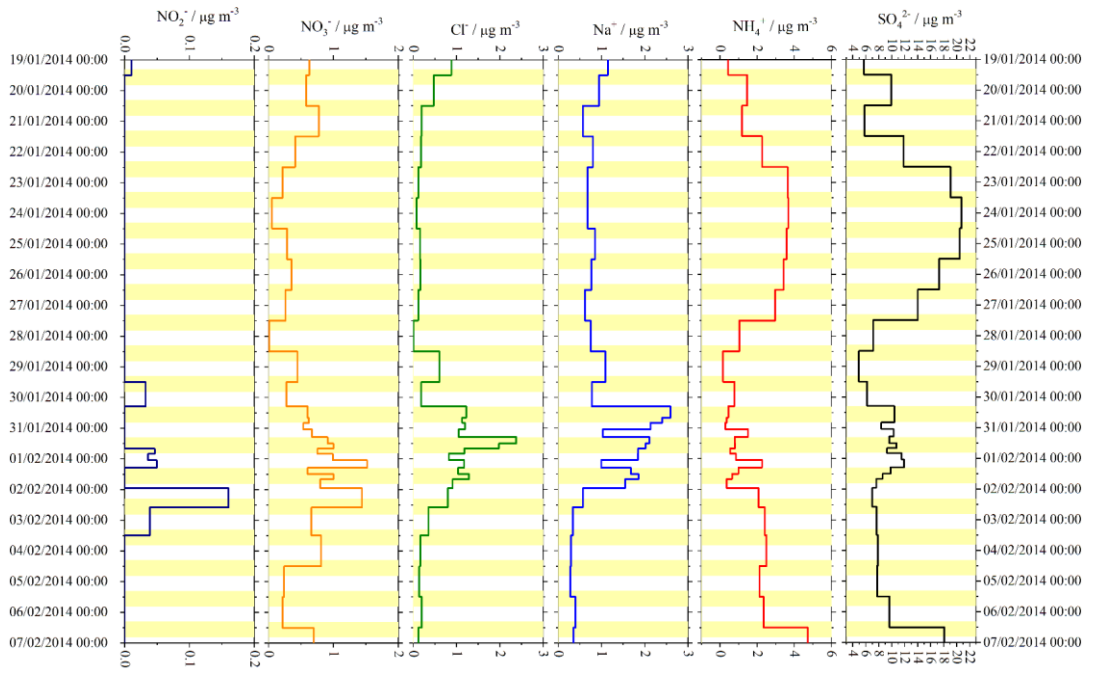
NO2- / µg m-3
NO3- / µg m-3
Cl- / µg m-3
Na+ / µg m-3
NH4+ / µg m-3
SO4 2- / µg m-3
19/01/2014 00:00
20/01/2014 00:00
21/01/2014 00:00
22/01/2014 00:00
23/01/2014 00:00
24/01/2014 00:00
25/01/2014 00:00
26/01/2014 00:00
27/01/2014 00:00
28/01/2014 00:00
29/01/2014 00:00
30/01/2014 00:00
31/01/2014 00:00
01/02/2014 00:00
02/02/2014 00:00
03/02/2014 00:00
04/02/2014 00:00
05/02/2014 00:00
06/02/2014 00:00
07/02/2014 00:00

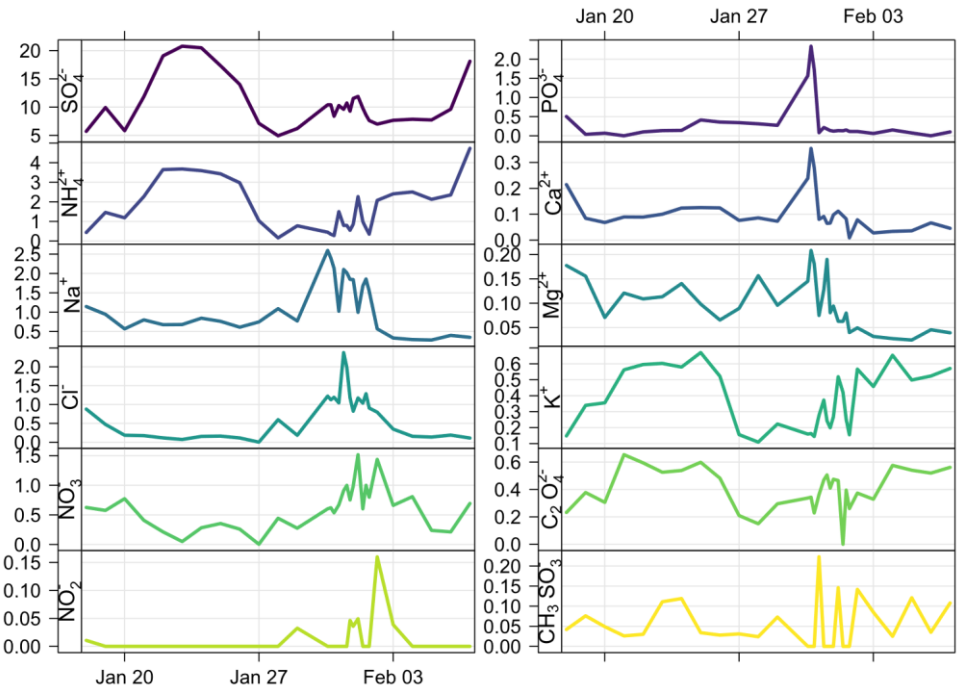

Figure 3: Time series of water-soluble ions ~~SO_4^{2-}, NH_4^+, Na^+, Cl^-, NO_3^- and NO_2^- concentration~~ (µg m^{-3}) measured during the Bachok demonstration campaign (18-01-2014 to 07-02-2014). ~~Yellow shaded areas represent the time between sunrise and sunset (local).~~

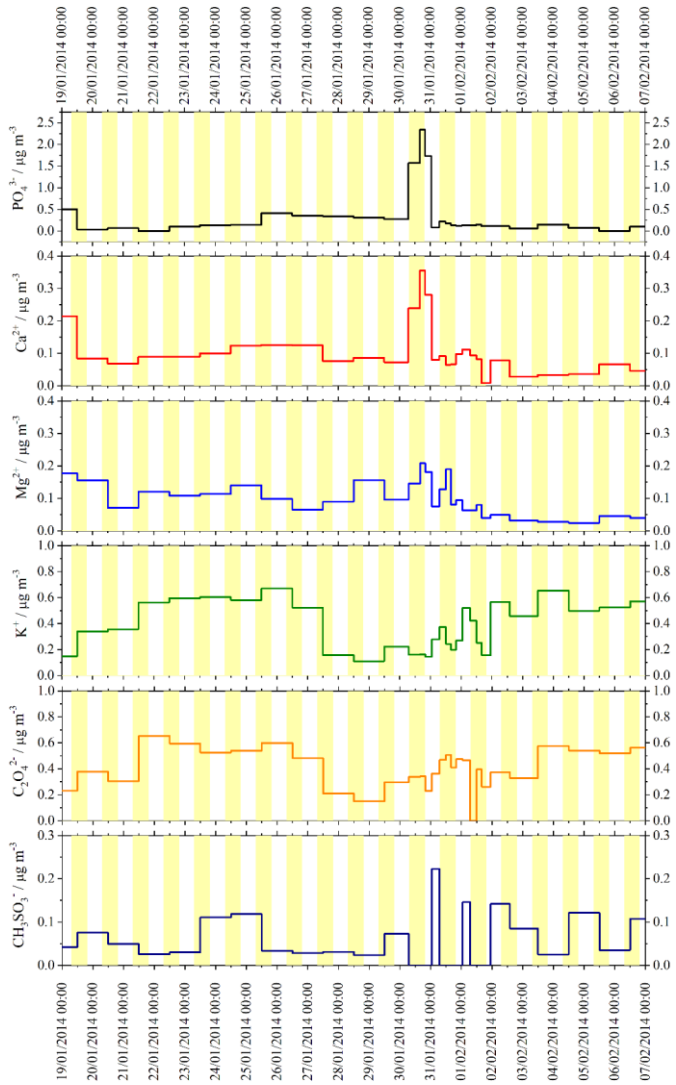

~~**Figure 4: Time series of PO_4^{3-}, Ca^{2+}, Mg^{2+}, K^+, $C_2O_4^{2-}$ and $CH_3SO_3^-$ concentration (µg m^{-3}) during the Bachok demonstration campaign (18-01-2014 to 07-02-2014). Yellow shaded areas represent the time between sunrise and sunset (local).**~~

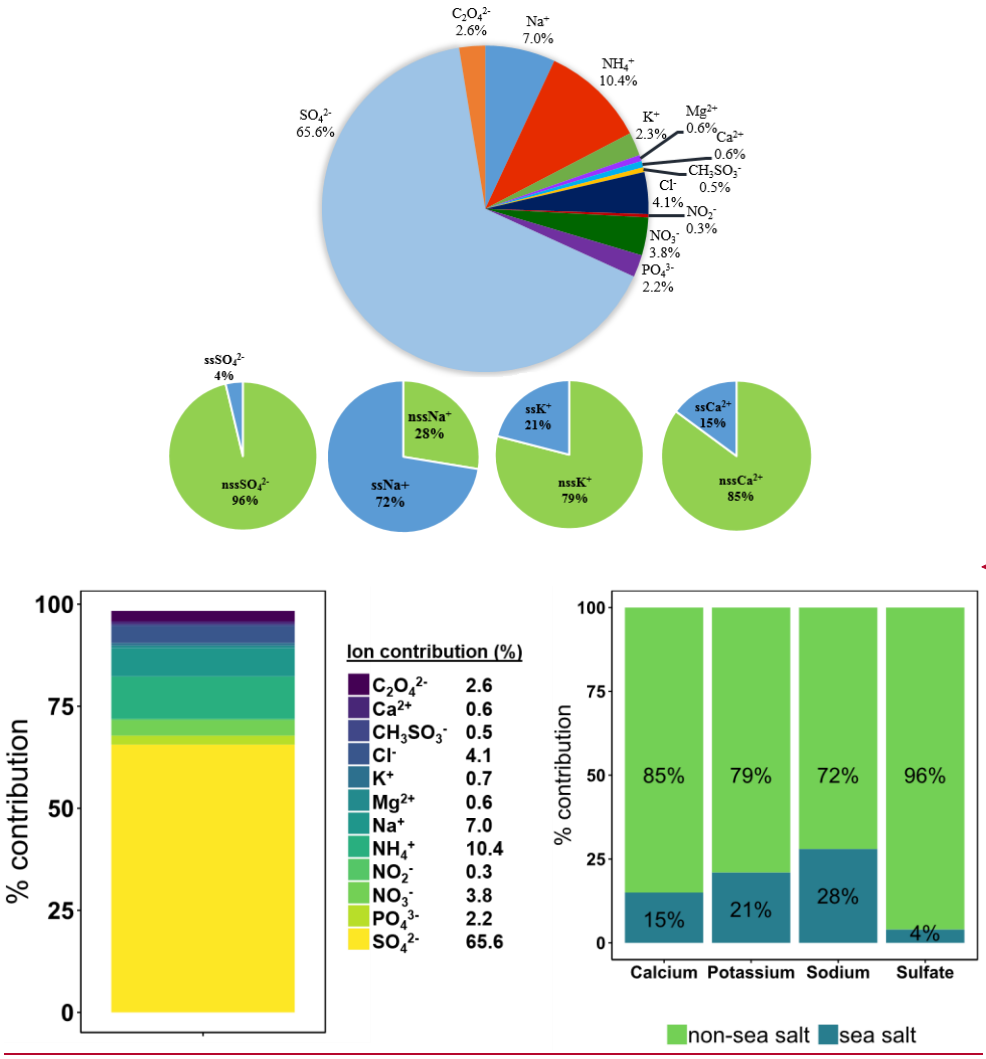

Formatted: Left

Figure ~~54~~: ~~Pie chart~~ Stacked bar chart to show the average mass composition of water-soluble ions in aerosol collected at the Bachok research station (~~upper~~ left panel) and ~~pie~~ stacked bar charts to show the percentage of non-sea salt and sea salt fractions of Ca_{ss}^{2+}, K_{ss}^{+}, Na^{+}, SO_4^{2-}, ~~K^{+}, Ca^{2+}~~ (~~lower~~right panel, left to right).

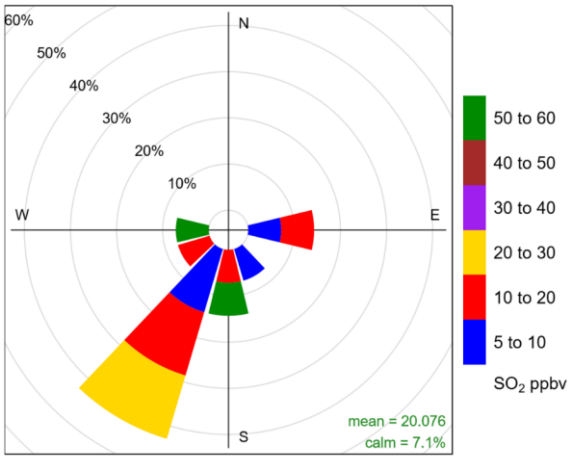

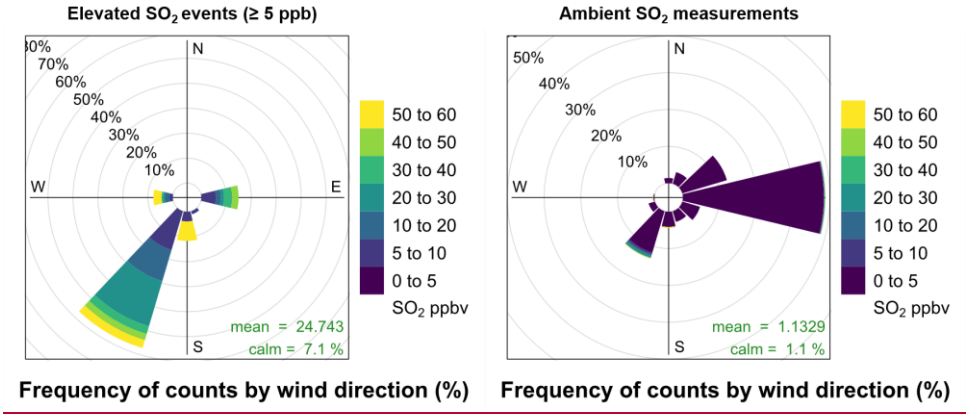

Figure ~~65~~: Pollution rose plots to show the relationship between wind direction and SO_2 concentration ~~(≥ 5 ppb)~~ at the Bachok measurement site. The left panel represents recorded SO_2 concentrations ≥ 5 ppb and the right panel represents all SO_2 data

Formatted: Superscript
Formatted: Superscript
Formatted: Subscript

recorded during the measurement period. Plot constructed using the openair package in RStudio (Carslaw and Ropkins, 2012; Carslaw, 2015).

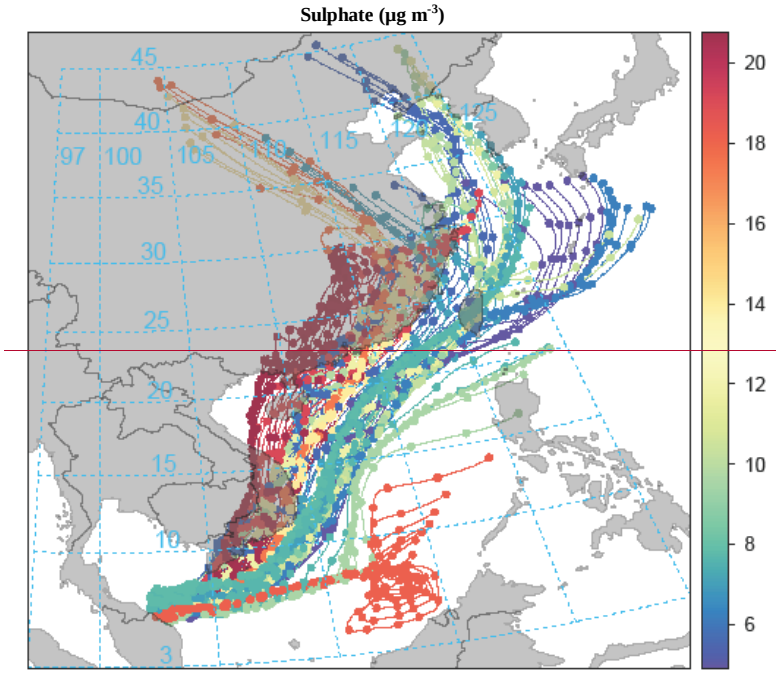
Sulphate (µg m-3)
45
40
97
100
105
110
115
120
125
35
30
25
20
15
10
3
20
18
16
14
12
10
8
6

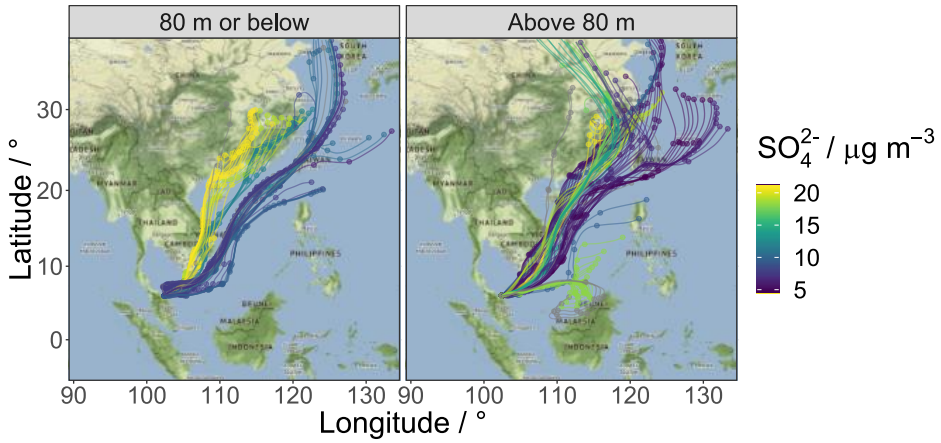

Figure ~~7~~6: 7-day HYSPLIT backward air mass trajectories centred on the Bachok research station between 18-01-2014 and 07-02-2014. The back trajectories are coloured by the concentration of SO_4^{2-} (μg m^{-3}). Trajectories with a mean height of 80 m or below are shown in the left panel and trajectories with a mean height greater than 80 m are shown in the right panel.~~Plot constructed using the openair package in RStudio (Carslaw and Ropkins, 2012; Carslaw, 2015).~~

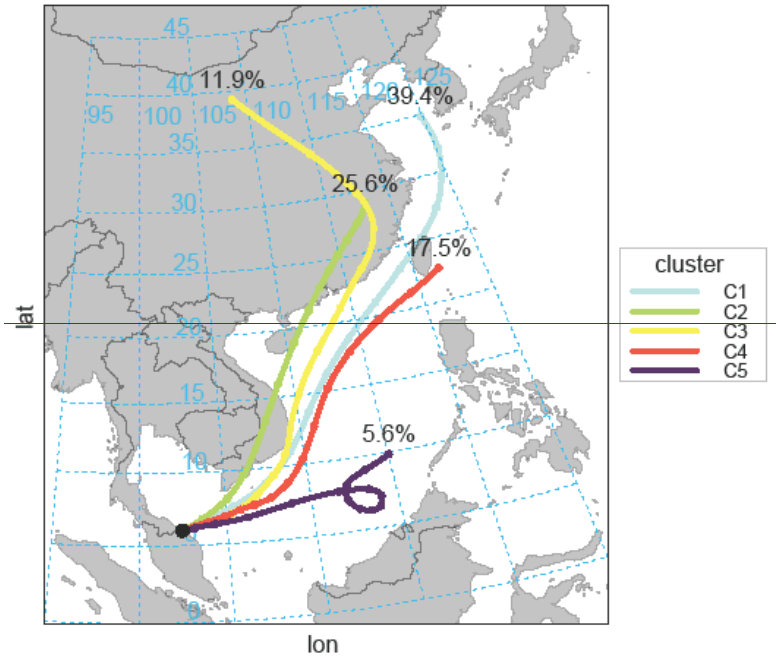

950

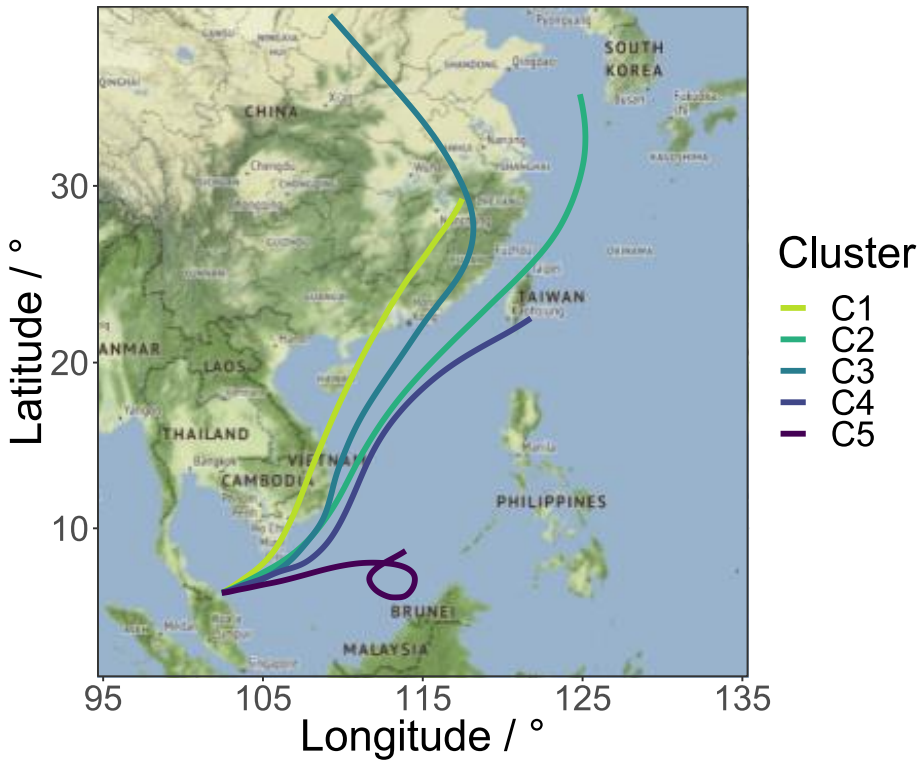

Figure 87: 5-cluster solution to backward air mass trajectories centred on the Bachok research station between 18-01-2014 and 07-02-2014. ~~**Plot constructed using the openair package in RStudio (Carslaw and Ropkins, 2012; Carslaw, 2015).**~~

955

Formatted: Normal, Left, Line spacing: single

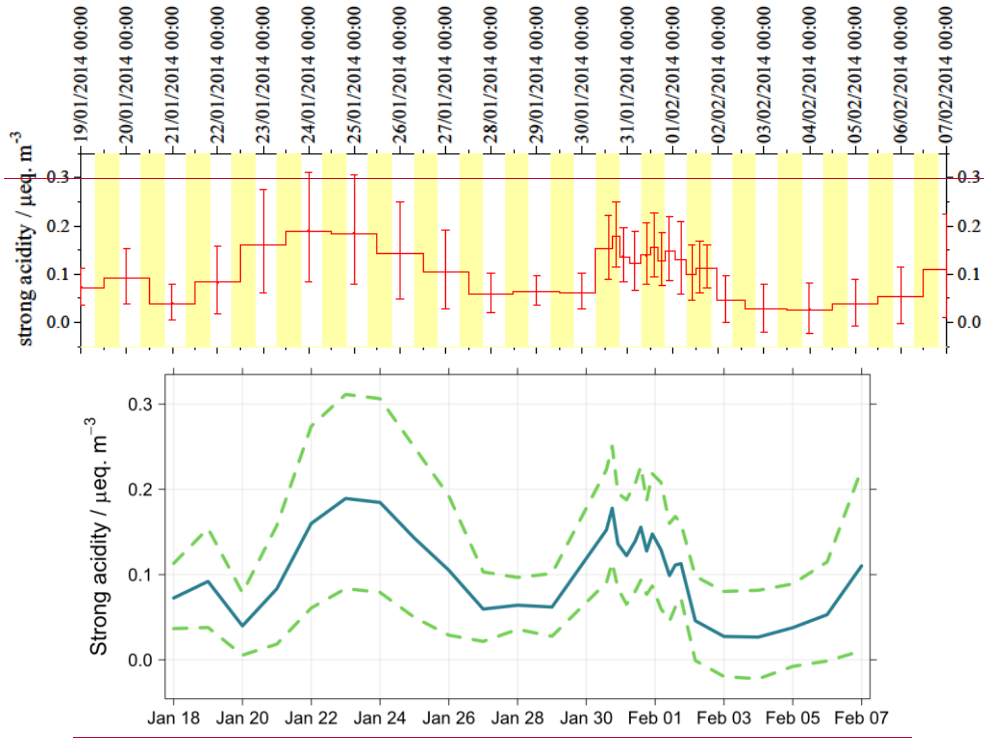

Figure ~~9~~8: Predictions of particle strong acidity for the aerosol collected during the Bachok measurement campaign. Dashed lines represent predictions of maximum and minimum limits of strong acidity. ~~Particle strong acidity and associated error predictions for the aerosol collected during the Bachok measurement campaign. Yellow shaded areas represent the time between sunrise and sunset (local).~~

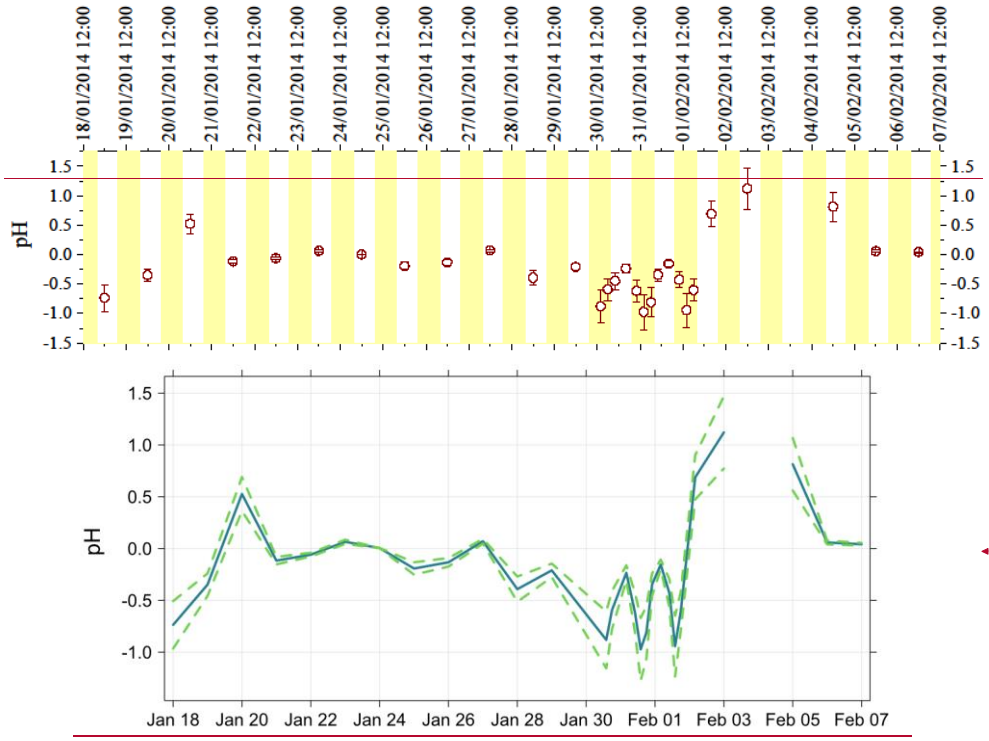

965 **Figure ~~10~~9: Predicted $PM_{2.5}$ pH at the Bachok measurement site using ISOROPPIA-II (Fountoukis and Nenes, 2007). Dashed lines represent predictions of maximum and minimum limits of pH.~~Predicted $PM_{2.5}$ pH at the Bachok measurement site using ISOROPPIA-II. Yellow shaded areas represent the time between sunrise and sunset (local).~~**

970

975

Formatted: Centered

Formatted: Subscript

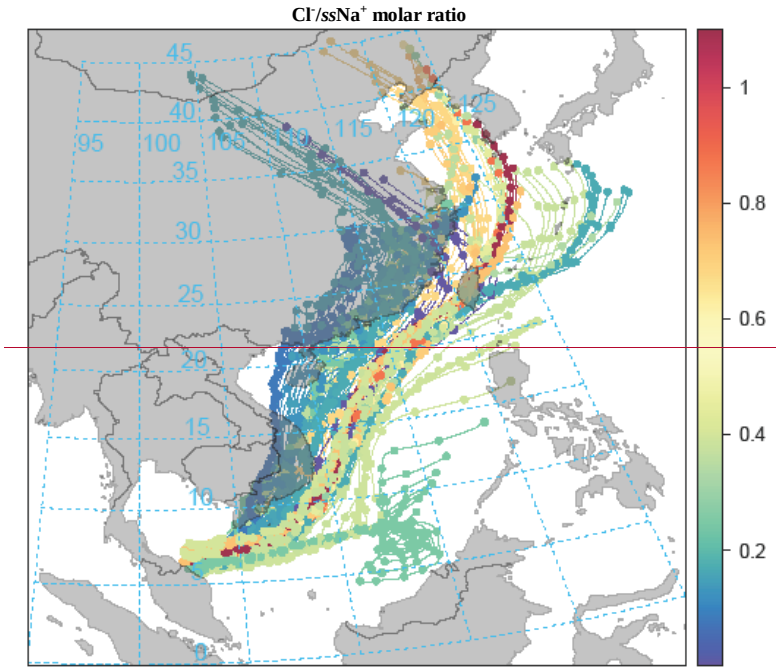
Cl⁻/ssNa⁺ molar ratio
45
40
35
30
25
20
15
10
95
100
105
110
115
120
125
1
0.8
0.6
0.4
0.2

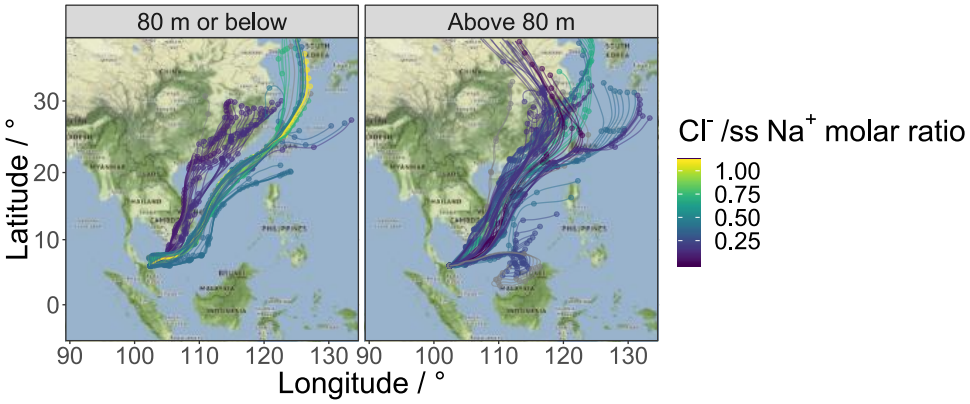

Figure 1011: 7-day HYSPLIT back trajectories centred on the Bachok research station, between 18-01-2014 and 07-02-2014. The back trajectories are coloured by the $Cl^-/ssNa^+$ molar ratio. Trajectories with a mean height of 80 m or below are shown in the left panel and trajectories with a mean height greater than 80 m are shown in the right panel. ~~Plot constructed using the openair package in RStudio (Carslaw and Ropkins, 2012; Carslaw, 2015).~~